Electronic Theses and Dissertations

8-2020

An investigation of the effect of contour process parameters on the surface roughness and dimensionality of overhanging features in 17-4 stainless steel.

Katherine Schneidau
University of Louisville

AN INVESTIGATION OF THE EFFECT OF CONTOUR PROCESS PARAMETERS ON THE

SURFACE ROUGHNESS AND DIMENSIONALITY OF OVERHANGING FEATURES IN 17-4

STAINLESS STEEL

By

Katherine Schneidau

B.S., University of Louisville, 2019

A Thesis

Submitted to the Faculty of

J.B. Speed School of Engineering, University of Louisville

in Partial Fulfillment of the Requirements

for the Degree of

Master of Science

in Mechanical Engineering

Department of Mechanical Engineering

University of Louisville,

Louisville, Kentucky

August 2020

AN INVESTIGATION OF THE EFFECT OF CONTOUR PROCESS PARAMETERS ON THE

SURFACE ROUGHNESS AND DIMENSIONALITY OF OVERHANGING FEATURES IN 17-4

STAINLESS STEEL

By

Katherine Grace Schneidau

B.S., University of Louisville, 2019

A Thesis Approved on

July 23, 2020

by the following Thesis Committee:

_____

Thesis Director
Dr. Thomas A. Berfield

_____

Thesis Co-Director
Dr. Thomas L. Starr

_____

Third Committee Member
Dr. Li Yang

ACKNOWLEDGEMENTS

I would like to thank Ed Tackett, Gary Graf, Tim Gornet, and Dr. Thomas Starr for the guidance and opportunities they have given over the past three years that has shaped my Additive Manufacturing knowledge base. To my thesis advisor Dr. Thomas Berfield, who has helped me throughout my thesis journey, especially the last few months of pushing forward to complete my thesis in time.

I would also like to thank my fellow cooperative engineering interns and graduate research assistants, Sean Dobson, Kayla Montgomery, and Justin Gilham for all their assistance over the past year while I completed my thesis.

To say this journey has not had its share of bumps would be an understatement, but one that I would never choose to go a different way. I have grown not only as a student and young adult, but as an emerging member of the Additive Manufacturing workforce, and I look forward to expanding my understanding of Additive Manufacturing for years to come.

Thank you.

ABSTRACT

AN INVESTIGATION OF THE EFFECT OF CONTOUR PROCESS PARAMETERS ON THE

SURFACE ROUGHNESS AND DIMENSIONALITY OF OVERHANGING FEATURES IN 17-4

STAINLESS STEEL

Katherine G. Schneidau

July 27, 2020

The relationship between varying contour settings and part geometry provides insight into the attainable surface roughness and dimensional accuracy of parts fabricated in 17-4 stainless steel via selective laser melting (SLM). Varying the contour settings of laser power (W), scan speed (mm/s), and beam offset (mm) for unsupported inclined bars. The utilization of a coordinate measuring machine (CMM) and surface profilometer quantified the dimensional accuracy and average surface roughness (Ra) for upface, downface, and topface surfaces. Adjusting the laser power and scan speed had minimal affect to surface roughness compared to part geometry. Part dimensionality was affected by the incline angle, laser power, and scan speed. Lower energy densities (J/mm) resulted in oversized parts, while higher energy densities resulted in undersized dimensions. A clear relationship between varying contour settings and part geometry with the dimensionality and surface roughness of 17-4 fabricated benchmark parts was found.

TABLE OF CONTENTS

LIST OF TABLES

LIST OF FIGURES

INTRODUCTION

PROBLEM STATEMENT/MOTIVATIONS

Additive Manufacturing (AM) is the next step in advancing the field of manufacturing by enabling the ability to achieve geometries not attainable through traditional subtractive manufacturing due to the layer-by-layer process of adding material rather than removing them. For over 25 years the Wohler's Report (Wohlers et al., 2018) has been following the trends of AM. In their 2018 report, Wohler Associates discuss the growth of AM products and services, which averaged a growth of 24.9% over the previous four years. In this paper, laser powder bed fusion (L-PBF) of metals is discussed with respect to the limitations and concerns for producing parts fabricated through this process, also called Selective Laser Melting (SLM). The main concern is how surface roughness and dimensionality of parts can be altered through changes to the process parameters (laser power, scan speed, beam offset). Additional concerns that can be evaluated further from the results of this experiment includes how parameter changes can affect part performance (fatigue properties) and post-processing operations, such as dimensional machining, and surface operations.

The importance of this research stems from how surface roughness has been found to affect the fatigue performance of parts. The consensus from a literature review of metal AM structure mechanical performance is clear: when there is a rougher surface, the likelihood of cracks propagating from the surface greatly increases. Gockel, Sheridan, Koerper, and Whip (2019) found such results for AM metal fatigue performance and noticed that for the right laser power and scan speed settings the surface roughness was controlled, reducing surface crack propagation. When the potential for surface crack propagation decreases, the primary initiator of fracture moves to the presence of sub-surface porosity or inclusions. Adjusting the presence of sub-surface porosity and decreasing the surface roughness of a part can contribute to a longer fatigue life.

As more research continues for SLM, trends between processing parameters and fabricated part quality will be further understood. Since there are over 3600 variables that can be adjusted to create an almost endless array of processing parameters, parameter development can be difficult. A parameter setting may produce excellent mechanical properties and build fast but come at the cost of surface finish or roughness.

The surface roughness of a selective laser melting (SLM) fabricated part is influenced by the overhang angles of the geometry, scan strategy (stripe, checkerboard, bi-directional/meander), and exposure settings (laser power, scan speed, hatch distance). This research will examine the relationship between surface roughness and part dimensionality for varying parameter settings. Understanding how to control surface roughness can help minimize crack propagation for fatigue property influence and part life (Solberg et al., 2019).

HYPOTHESIS/APPROACH

The focus of this research is on the relationship between contour parameter settings such as laser power, scan speed, and beam offset on the surface roughness and dimensionality of overhanging features. From previous work in SLM research, surface roughness has been found to be adjusted by process parameters, part geometry, and scan strategy. This study will focus on the contour settings, of various inclined bars with holes. The benchmark part described in Section 3.1 was created to quantify the effect of unsupported overhanging angles, concave, and convex holes on surface roughness and dimensionality for varying contour settings.

It is expected that adjusting the laser power and scan speed of the contour will either decrease or increase the surface roughness as the overhanging bars move down from 90° to 30°, relative to the build plate surface. Specifically, increasing the energy that goes into the material upon scanning will adjust the melt pool size and subsequently the surface roughness and dimensionality. The beam offset of the contour settings will control the dimensionality of the final part, with increasing the beam offset resulting in a larger part than the supplied CAD.

Through the literature review it is clear there is a relationship between surface roughness and dimensional accuracy with varying parameter settings for different materials. While materials such as Ti-6Al-4V and 316 SS have been much studied, there is little research published on these relationships for 17-4 stainless steel, specifically when looking at the contour or outline settings. The goal of this research is to

establish a relationship trend of the dimensionality and surface roughness of various overhang geometries for 17-4 stainless steel with contour parameter settings for parts fabricated by the Selective Laser Melting (SLM) process.

OVERVIEW OF WORK THESIS

All work has been divided into multiple sections to ensure clarity. In the next section, Section 2, an overview of the current state of knowledge in the AM metal field is presented along with reviews of previous studies that explore the influences on surface roughness and dimensionality. The literature review is broken into sub-sections that evaluate the effect a single variable has on surface roughness and dimensionality from part geometry, scan strategy, and parameter values. Section 3 contains the experimental approach and includes the equipment used, material, and the parameter settings for each specimen built. Section 4 contains a report and analysis of dimensionality and surface roughness testing of each specimen with all conclusions stated in Section 5. Mechanical testing was not included in this analysis due to time constraints, however it would be beneficial to include in future work.

LITERATURE REVIEW

SURFACE ROUGHNESS

EFFECTS OF PART GEOMETRY

Research on relationships between process parameters and surface roughness has been conducted on multiple other material systems from Inconel 718 and 316 stainless steel to Ti6Al-4V. Adjusting either laser power, scan speed, or hatch spacing can change an excellent mechanical property to excellent surface finish, but adjusting the values result in the presence of sub-surface porosity to increase or parts being less dense as the focus is to have high quality looking parts. Each material has different relationships with parameter settings, and a range of setting combinations result in optimal part quality in terms of density, surface roughness, and mechanical properties. Changes to each will get you "too cold", "too hot" or "just right" part quality depending on if you prefer mechanical property, surface finish, or density characteristics. With over 3600 combinations for scan speed and laser power settings along, utilizing an artificial neural network can help run simulations, and will allow a process map to be used for determining good parameter windows (Tran & Lo, 2019). These simulations have an algorithm that is developed based on the fabrication of samples and inputting the relationships found between variables such as laser power, scan speed, hatch distance, and scan strategy. The development of these neural networks take time to develop as there they are based upon examining the variable relationships through fabrication first. **Figure 1** shows a process map of 316L stainless steel used to determine optimal parameters to maximize density and reduce surface roughness.
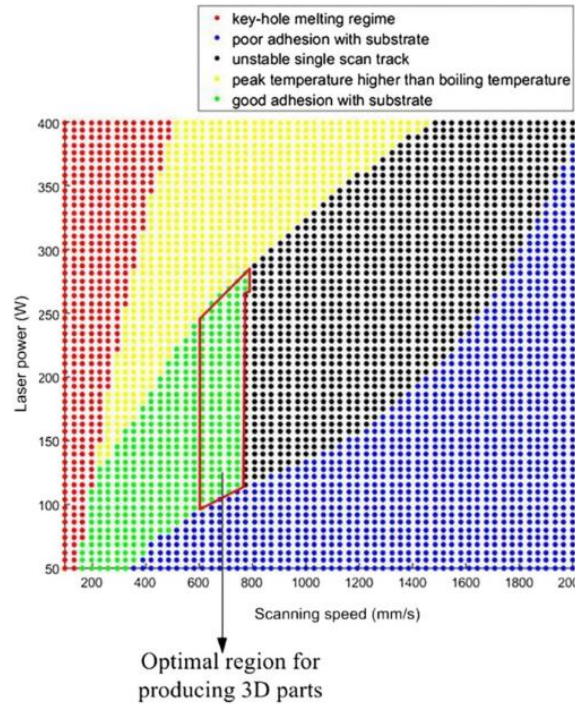
Figure 1. Process map of simulated parameter settings for 316L stainless steel utilizing constraints (Tran & Lo, 2019).

As seen in **Figure 1**, the 316L stainless steel (SS) material has a specific window that is simulated to produce near the maximum density (shown in green), and slight changes to the process parameters can result in defects or less dense parts (non-green colors). This relationship can be used to help determine process parameters for optimal surface roughness or mechanical properties.

As most parts will not be solid blocks but have areas of curved surfaces or complex surfaces, several experiments and analyses has been conducted on different materials to investigate the effects of varying overhang structures. One such study (Ni, Shi, & Liu), examined the effects of incline angles, between 0° and 90° from the build plate surface, on surface roughness and corrosion properties for 316L SS. Specifically looking at surface roughness, this research found that increasing the incline angle caused surface roughness. For all the angles tested, the process parameters were constant, allowing the focus to be on the effect of incline angle. **Figure 2** shows the average roughness (*Ra*) measurement along the top surface in two directions, parallel and perpendicular to the scan layer. To maintain a constant nomenclature the inclination angles used in this publication would align with the top surface values for the degrees listed, becoming 180°, 150°, 135°, 120°, and 90°.

5
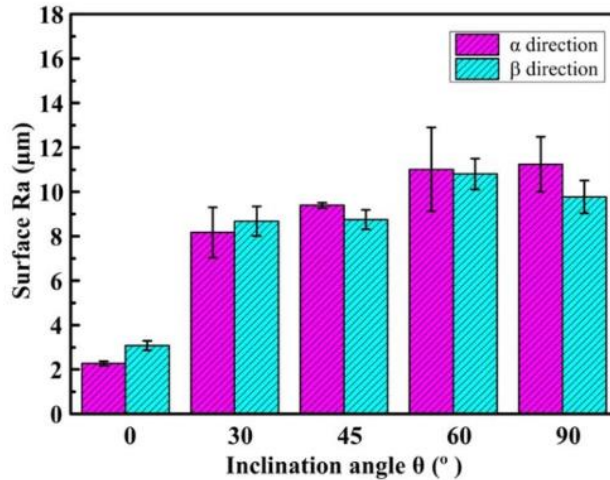
Figure 2. Average surface roughness (*Ra*) of the incline angles' top surface parallel (*β*) and perpendicular (*α*) to the scan direction for 316L stainless steel (Ni et al., 2019).

Shi, Wang, Liu, and Han (2019) also examined 316L SS overhangs, going a step further examining a chrome nickel alloy. The layer thickness varied between the two materials along with the incline angles between 15°-75°. Both materials followed the same trend as **Figure 2**, with surface roughness increasing as the incline becomes closer to parallel with the build plate. Klingaa, Dahmen, Baier, Mohanty, and Hattel (2020) examined the surface roughness of interior cooling channels fabricated in 17-4PH SS. In terms of application, having a smooth inner channel is important to maintain proper flow through the part, and because these interior channels cannot be easily subjected to post-fabrication surface processing. The circular channels were set at seven different inclination angles from 0°- 90° at constant exposure settings and a regression model was created to predict the *Ra* for each angle. Once again, this experiment demonstrated there is a strong dependence of surface roughness on inclination angle. It was also noted that the point of each channel with the highest *Ra* value was the top of the circle, which was expected as it is the highest unsupported point of the channel.

Reactive materials such as titanium and aluminum also have the surface roughness and incline angle trend shown by the non-reactive materials such as 316L SS, 17-4PH, and chrome-nickel alloy. Between the reactive and non-reactive metals there should be differences in the values of surface roughness as each material has an optimal parameter set. If the same settings were used for both material types, there would be

differences in the resulting surface roughness due to the effectiveness of the parameter set melting and fusing the material.

Taking a slightly different approach, Subbaian Kaliamoorthy, Subbiah, Bensingh, Kader, and Nayak (2020) included support structures in their analysis. Utilizing AlSi10Mg with varying exposure settings, it was found that the surface farthest from the front of the machine and perpendicular to the recoater (back surface) had a lower surface roughness value than the front surface due to the presence of overhangs and supports. **Figure 3** shows a schematic of the benchmark part with face nomenclature, with the front surface parallel to the recoater blade, away from the dispenser.
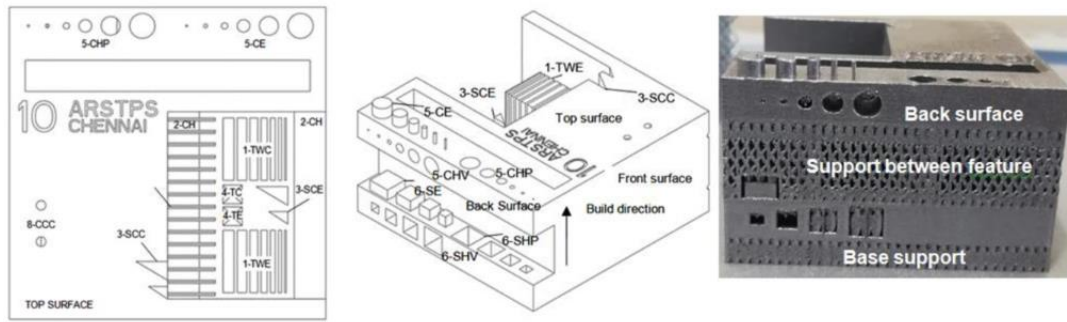
Figure 3. Geometry and surface notation of fabricated benchmark part (Subbaian Kaliamoorthy et al., 2020).

When discussing the surface roughness of the produced benchmark part, the Ra value was higher for the front surface followed by the top surface. The values of the Ra , the average maximum roughness peak (Rz), and the root mean square height (Sq) are shown in **Figure 4**Error! Reference source not found.**.**

Taylor Hobson profilometer	R_a [μm]	R_z [μm]	Sq [μm]
Surface			
Front	0.9045	3.6456	7.7698
Back	0.3824	1.9212	6.9743
Top	0.4879	2.2114	15.4683

Figure 4. Surface Roughness measurements for benchmark part in terms of surface plane (Subbaian Kaliamoorthy et al., 2020)

The reason for the back surface having the lowest roughness measurements was due to the plane features being supported, which minimized the fusion of un-sintered powder to the features. This analysis

demonstrated that surface roughness variation can occur for different geometries. Each of these experiments concluded with the same results, increasing incline angles towards 0° horizontal will increases surface roughness. This relationship is independent of material used as surface roughness values increased for low incline angles in four different materials.

The statement that surface roughness values increase as an incline angle decreases is further supported by research completed by Fox, Moylan, and Lane (2016). In this analysis the relationship between surface roughness and an overhang geometry for 17-4 SS was evaluated using varying laser power and scan speed. What was found is a dependence of the *Ra* value on the overhanging angle. As the angle decreased to 30°, the *Ra* value increased for all contour laser power and scan speed settings, shown in **Figure 5**. A relationship between incline angle and *Ra* is clear, but another occurrence to not is how each contour set results in a larger *Ra* measurement range as the incline angle decreases to 30°.
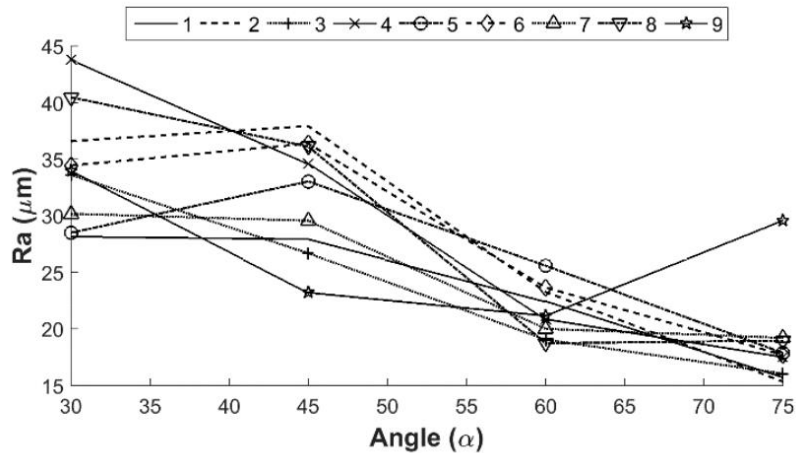
Figure 5. *Ra* of overhang angles 30°, 45°, 60°, and 75°. (Fox et al., 2016)

EFFECTS OF VARYING SCAN PATTERN STRATEGIES

The pattern in which a layer is scanned is important to the mechanical properties. Three types of strategies appear throughout several published papers and are bi-directional/meander, chess, and 67° rotational stripe. DePond et al. (2018) examined these three strategies utilizing solid cubes and hollow cubes to evaluate geometry, fabricated out of 316L SS. The goal was to examine how the scan strategies effect the surface quality using height maps of the scanned layer. This paper held constant parameter values for laser

power, scan speed, and hatch to focus on the effects of the scan path. **Figure 6** shows a height map for the bi-directional and 67° rotational stripe strategies on the solid cube and the strategy path while **Figure 7** shows the difference in surface roughness for the two strategies on a layer base.
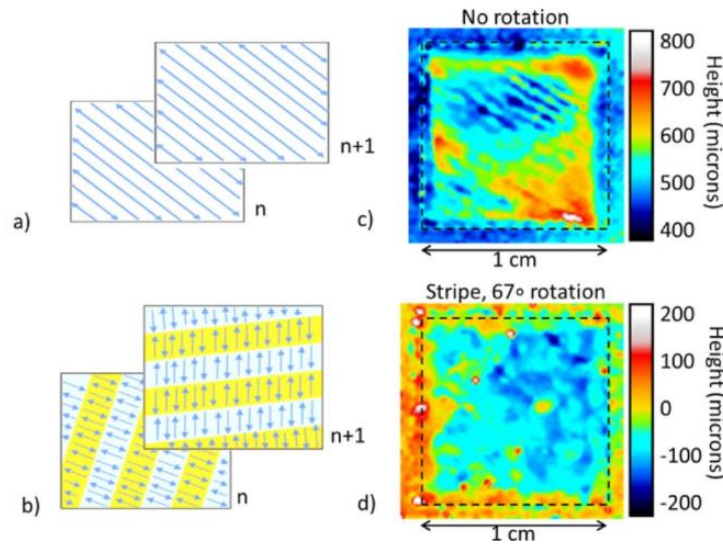
Figure 6. a) Path lines for bi-directional scan. b) path line for a 67° rotational stripe. c) height map for no rotation, bi-directional scan and d) height map for stripe path with rotation (DePond et al., 2018).
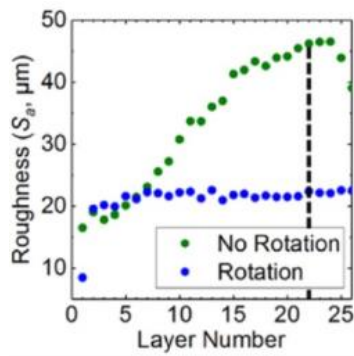
Figure 7. Surface roughness values, taken at each layer, with and without a 67° rotational stripe (DePond et al., 2018).

In **Figure 6** there is a black dotted outline for (c) and (d), that show the dimension of the cube. The bi-directional or no rotation scan has larger height deviations than the 67° rotated strategy which ties into the conclusion for surface roughness and helps confirm the trend shown in **Figure 7**. By rotating the scan path 67° between each layer, surface roughness is reduced and held close to 20μm.

A prior study conducted by Shi et al. (2019) discussed geometry analysis. This same study also examined the chess, meander, and 67° rotational stripe scan strategies for their blocks fabricated in 316L SS and a chrome-nickel alloy. What was found was that the chess and meander strategies produced low surface roughness for the chrome-nickel alloy while the stripe produced low surface roughness for 316L SS. The chess pattern is suitable for incline angles near perpendicular to the build plate. Meander and stripe are suitable for incline angles closer to parallel with the build plate. Overall, the scan strategy can affect the surface roughness and optimal strategies can differ between materials.

EFFECTS OF VARYING EXPOSURE SETTINGS ON SURFACE ROUGHNESS

The exposure variables include laser power, scan speed, and hatch distance, each having their own relationship with surface roughness. These settings can be used to create exposure strategies such as fill, up-skin, downskin, and contour. **Figure 8** demonstrates the naming nomenclature for surfaces at an incline, along with where each strategy is activated for a given layer slice for the overhang geometry.

DePond et al. (2018) adjusted the top surface or up-skin laser power to surface roughness changes. This paper also utilized a different measurement method called spectral domain optical coherence tomography (SD-OCT). The SD-OCT collects surface topography through reflected light off the scanned layer. **Figure 9** shows the changes in surface roughness when altering the up-skin laser power.
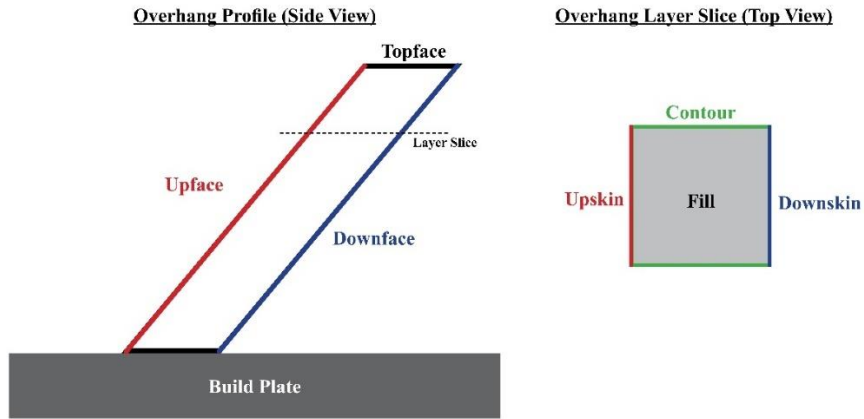
Figure 8. Overhang part surface nomenclature and layer slice denoting the activation areas of different exposure settings.
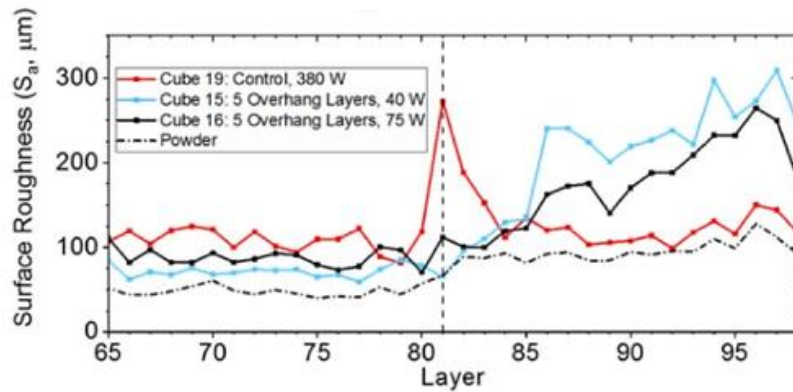
Figure 9. Arithmetical mean height (*Sa*) of top surface of hollow cube with different laser powers for up-skin and downskin on overhang layers (DePond et al., 2018).

Increasing the laser power of the top surface results in re-melting the top several layers based on the input energy. The trend shown in **Figure 9** shows that increasing the upskin laser power increases the surface roughness. Shi et al. (2019) found similar results adding that increasing the number of scans will decrease roughness, as the layers are re-melted.

Deng, Mao, Yang, Niu, and Lu (2020) utilized a design of experiments software to determine the optimization of laser power, scan speed, and hatch distance of 316L SS. Building samples in a range of exposure settings, it was clear that laser power had a significant effect on surface morphology as shown in

Figure 10. Unlike laser power and scan speed, the hatch distance did not have a significant effect on surface roughness. Tran and Lo (2019) confirmed the strong relationship between surface roughness, laser power, and scan speed through their finite element analysis and artificial neural network analysis of over 3600 combinations of exposure parameters. The analysis concluded that a low scan speed increased surface roughness and for the 316L SS material, and process map shown in **Figure 1**, where the optimal surface roughness and density range is outlined. Since the main objective of the paper was to maximize density, there is reason to believe that the optimized parameters selected in **Figure 1** can be altered if the focus was on surface roughness.
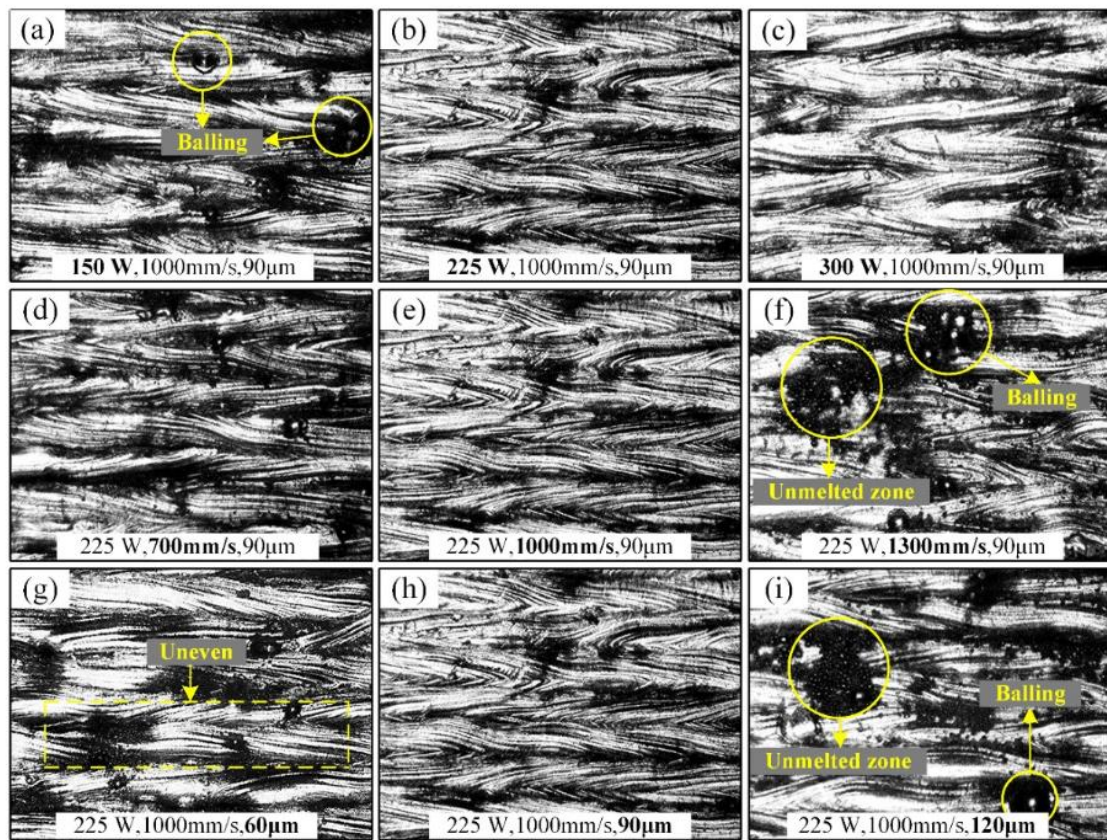
Figure 10. Surface morphology of parts built at varying laser power, scan speed, and hatch distance (Deng et al., 2020).

Referring to the work mentioned in SURFACE ROUGHNESS, authors Fox et al. (2016) found a relationship between the part geometry and surface roughness, however another scope of the work was to determine a connection between surface roughness and the contour parameters. After analyzing the data, the

authors cited that a clear connection between the *Ra* and the parameters could not be found with the angled blocks fabricated, calling for a feature based part to examine the connection.

DIMENSIONALITY

Dimensionality as the focus of research is limited in published work. Instead dimensional accuracy is a supporting subject used to help well-round experimental analysis. The National Institute of Science and Technology (NIST), while organizing and determining how to control variability in part quality, gathered the few published work to discuss what inputs affect the dimensional outcome of parts (Mani, Lane, Donmez, Feng, & Moylan, 2017). Dimensional accuracy and tolerance are not the focus of the review, but the knowledge presented supports the scope of controlling part quality for powder bed fusion part fabrication.

Within the review it was stated that process parameters were the "inputs" that are the main factor in the amount of energy that is sent to the powder and the resulting interaction. From that statement manipulations to the process parameters will affect the resulting part, what the specific results are determined by experimental analysis. The review included the work completed by Delgado, Ciurana, and Rodríguez (2012) on dimensionality of metal parts. The results concluded that the build direction can affect the dimensional accuracy of parts. The review also included the work by Wang, Yang, Yi, and Su (2013) that specifically examined the quality of overhanging surfaces, finding that control over a part orientation and the energy input into the material will affect the quality. Better control and optimization with improve quality of overhanging surfaces.

The work completed by Calignano, Peverini, Addamo, and Iuliano (2020), while not cited in the NIST review due to publication time, demonstrated the effect of reducing the radius of an internal channel. Utilizing a constant core and contour parameter setting, denoting the values assigned for upskin and downskin laser power and scan speed, the authors found that as the radius decreased from 50 mm to 30 mm, deviations did as well. The deviations were averaged across the twisted internal channels. The measured values were verified through calculations determining the deviations to not be a result of layer lines. In their conclusion Calignano, Peverini, Addamo, and Iuliano (2020) cited that a compensated CAD should be used to accuratedly fabricate parts after an optimized parameter set has been created.

EXPERIMENTAL SETUP

BENCHMARK PART

A single part was designed to include all tested geometries to limit the number of parts to fabricate. Two versions of the benchmark part were used. The first version, v1, had solid overhang bars for 30°, 45°, 60°, 75°, and 90°. The final version, v2, was larger in overall size to ensure adequate surface area for testing the surface roughness and included three feature sizes to measure convex and concave radii. The two different geometries are shown in **Figure 11** with their overall dimensions shown in **Table 1**.

(a)   (b)
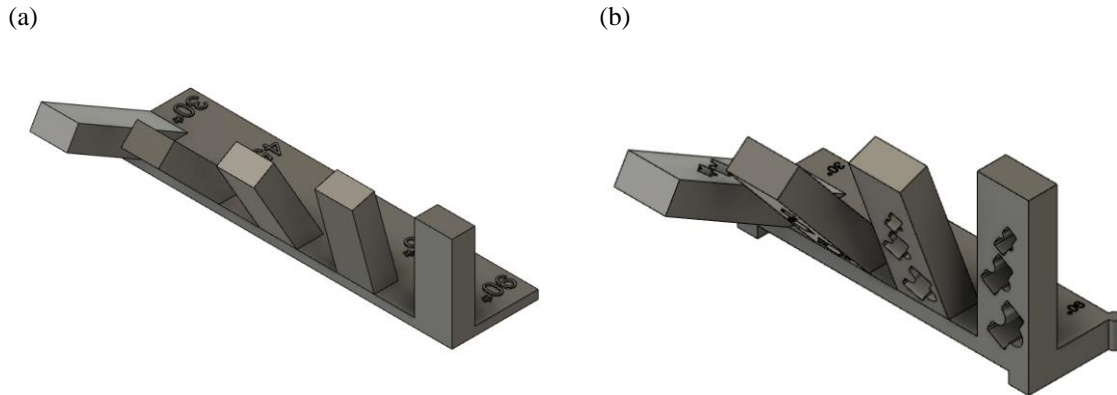
Figure 11. Benchmark geometry of (a) v1 and (b) final version, v2.

Table 1. Benchmark Part dimensions

Version	Overall Dimension (mm)	Overhang Values	Overhang 'Block' Dimension (mm)	Hole radii (mm)
1	60.5 x 15 x 17	30°,45°,60°,75°,90°	15 x 4 x 6.5	-
2	102 x 30 x 55	30°,50°,70°,90°	50 x 10 x18	1, 2, 3

MACHINE SETUP

An EOS M290 Direct Metal Laser Sintering (DMLS) machine was utilized for all part fabrication. A ceramic rigid recoater blade was used for all testing, and the material was 17-4 SS. Initial testing with version 1 of the benchmark part was completed for contour sets 1 and 2 to examine the effect of beam offset. The final test geometry was built for contour sets 2-5. Both parts were fabricated with a constant fill parameter set and strategy pattern. Only the beam offset, laser powers, and scan speeds were adjusted for the different contour parameter sets. All tested values for each variable are shown in **Table 2.** A single contour line was utilized with the laser completing two passes along this line. If two contour lines were utilized then a beam offset could be assigned to each line. The upskin laser power and scan speed are activated when an area of the layer will not be scanned on the next layer. The downskin settings are activated for the opposite when the area below the current section was not scanned. This event is expressed graphically by **Figure 8**.

Table 2. Parameter values

Set No.	Laser Power (W)			Scan Speed (mm/s)			Beam Offset (mm)
	Standard	Upskin	Downskin	Standard	Upskin	Downskin	[line 1, line 2]
1	60	60	40	700	700	700	0.02, 0
2	60	60	40	700	700	700	0.1, 0.08
3	120	120	120	700	700	700	0.1, 0.08
4	60	60	40	350	350	350	0.1, 0.08
5	120	120	120	1400	1400	1400	0.1, 0.08

QUANTITATIVE ANALYSIS

SURFACE ROUGHNESS

A Mitutoyo SJ-210 surface profilometer was used to measure the surface roughness of the specimen for both planes and holes. A 0.75mN, diamond tip gauge detector was used for all measurements. The stylus profile includes a tip radius of 2μm and tip angle of 60°. A custom apparatus was created to hold the profilometer along the measured surfaces to ensure repeatability. The profilometer was held perpendicular to the measure surface for the duration of each measurement, but the "caps" ensured the profilometer was perpendicular to the surface and would not move once testing began**.**

Data was recorded and output into a certificate presentation using Surftest, the software created by Mitutoyo for surface profilometer testing.

Table 3 shows the constant setting in which all surface roughness measurements were taken at, including the filter, cutoff length (Lc), and sample length (Ls).

Table 3. Surface Profilometer settings

Standard	ISO1997
Profile	R
Filter	Gauss
Ls	2.5 µm
Lc	0.8 µm
N	8

A specific nomenclature was used to quantitatively classify the upface, downface, and topface surfaces for analysis, specifically for surface roughness. The assigned incline angle was determined based upon the direction of the surface measurements were taken. A visual for surface angles is shown in **Figure 12** and **Table 4** shows how the surface angles are classified in this analysis.

Table 4. Nomenclature for surface angle based upon surface location and overhanging bar incline angle.

Overhang Bar	Upface	Downface	Topface
90	90°	90°	180°
70	120°	70°	160°
50	150°	50°	140°
30	180°	30°	120°
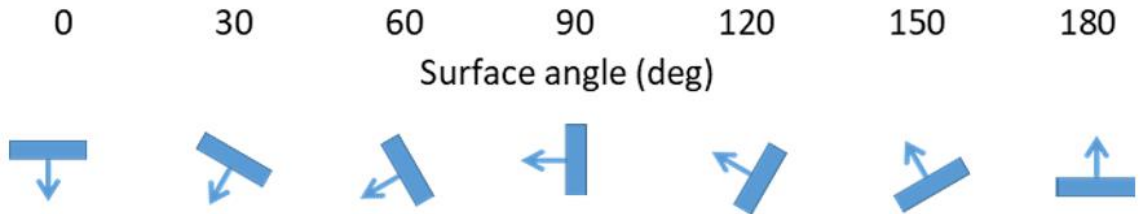
Figure 12. Standard nomenclature for part surfaces based on the incline angle from the build plate top surface.

The hole features were labelled differently as two types of surfaces were generated, concave and convex, each at three different radii. A total of four measurement location were established for each surface type that correlates to the surface measurement nomenclature shown in **Figure 12**. The general measurement area for the hole features are shown in **Figure 13**.
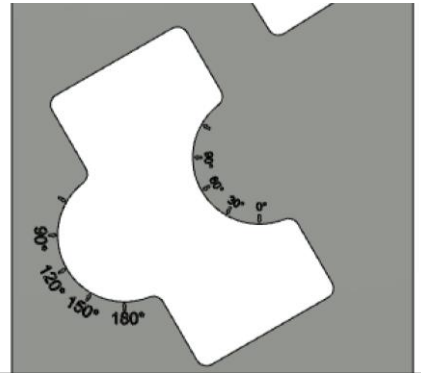
Figure 13. Measurement locations for concave and convex hole features on each overhanging bar, denoted in the surface angle nomenclature presented in **Figure 12**.

DIMENSIONALITY

To measure the dimensionality of the as-built samples a CMM was programed. Utilizing a Renishaw PH10T probe with a 1mm diameter ruby tip on a Brown & Sharpe One CMM, a program was designed in Nikon CMM-Manager Software. The program included measurements of the thickness and width of each overhang bar, and the radius of each hole created through the bars. A report for each bar was output at the end of the program to denote the measured values and the deviation from CAD values. The dimensionality was tested to examine the effects of adjusting the contour laser power, scan speed, and beam offset values.

17

The beam offset was examined through measuring the v1 overhang specimen, and the laser power and scan speed were examined with the v2 specimen.

Due to the research timeline, the v1 overhang specimen was measured with digital calipers, which take the measurement of highest peak to highest peak. The CMM measurements are point based with a round probe tip, resulting in the potential for measurements to be made on a peak or valley on the part surface. A difference in tolerance from each measurement method should be noted with claimed accuracy of the CMM to be 1 micron or 0.001 μm while it is unreasonable to claim accuracy that small for a digital caliper. Since the beam offset settings of the v1 benchmark part is to examine the overall dimensions of each bar to compare to the CAD, the digital caliper results are adequate. However, any attempts to compare the results of the v1 and v2 benchmark parts will need to maintain knowledge of the two different tools used to measure the part dimensions.

DIMENSIONALITY

EFFECT OF VARIATION IN LASER POWER AND SCAN SPEED

The CMM program allowed for the thickness and width of each overhanging bar to be measured. In terms of the measured surface and inclination angle there is a correlation between the incline angle and the thickness CAD deviation. **Figure 14** shows the measured thickness and width of each incline bar for contour sets 2-5. Each contour set is denoted by their laser power (W) and scan speed (mm/s) settings and the CAD or nominal value is denoted. The thickness is measured as the difference between the upface and downface, while the width is the cross-section between the two planes.

(a)

(b)
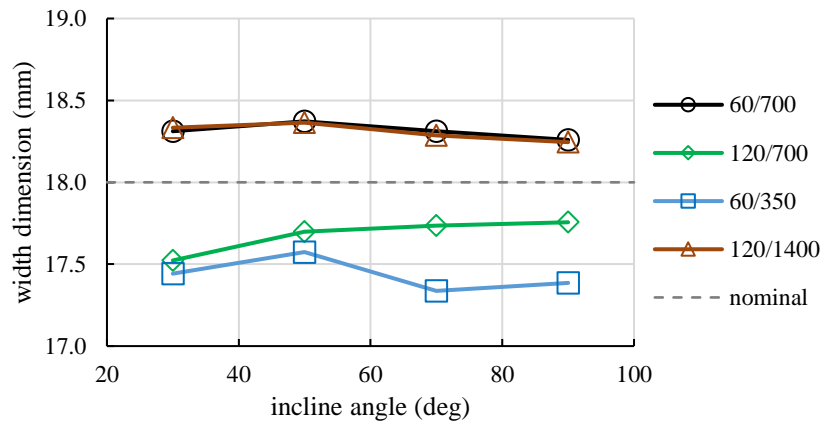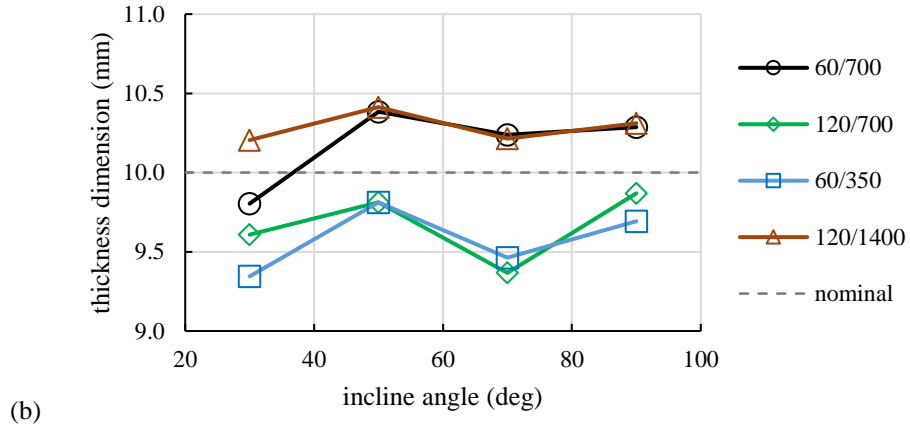
Figure 14. (a) measured width and (b) measured thickness of the v2 overhanging bar for varying laser power and scan speed settings correlating to contour sets 2 through 5.

From the data a clear separation is shown between two groups of laser power and scan speed values. This separation can be attributed to energy density values or result from the four samples being split between two builds and the two different energy densities 0.086 J/mm (top group) and 0.171 J/mm (bottom group). The thickness measurement also demonstrated, specifically for the v2 specimen, that as the incline angle decreases to 30° that the downskin plane is not flat, and sags as shown in **Figure 15**. This result occurred for all four v2 benchmark specimens but was prominent for the contour sets 2 and 5. There was also discoloration in each sample that looked as if the samples burned which was determined to be a result of the part geometry and lack of heat dissipation during fabrication.

(a)   (b)   (c)   (d)
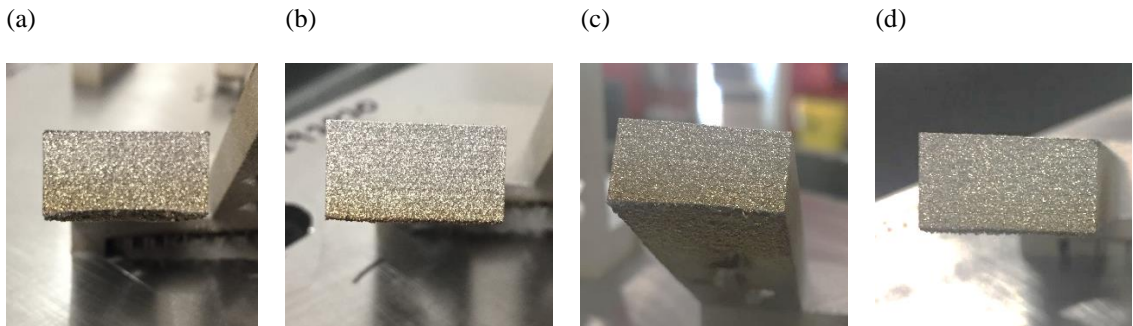
Figure 15. 30° downskin sagging for (a) contour set 2 (b) set 3, (c) set 4, and (d) set 5.

The CMM measurements were able to verify that as the incline angle decreases to 30°, downfacing surfaces increase their distance from 0mm or flat shown in **Figure 16**, with a larger sagging effect for some

of the contour settings. This is also shown through a color gradient point cloud measurement for each overhang bar. Each incline value and the color gradient for each surface is shown in **Figure 17**. The color gradient is broken up to the cooler colors demonstrate expansion, such as sagging, while the warm colors express contraction. The expansion effect is reversed when the incline angle is increased toward 90°, demonstrated by the shrinkage of the topface, similar to a meniscus shown in **Figure 17**. This behavior occurs for contour sets 2 through 5 and the reports for each benchmark specimen fabricated are shown in Appendix A (**Figure 22-25**) along with the flatness report for each contour setting and overhang bar (Table.
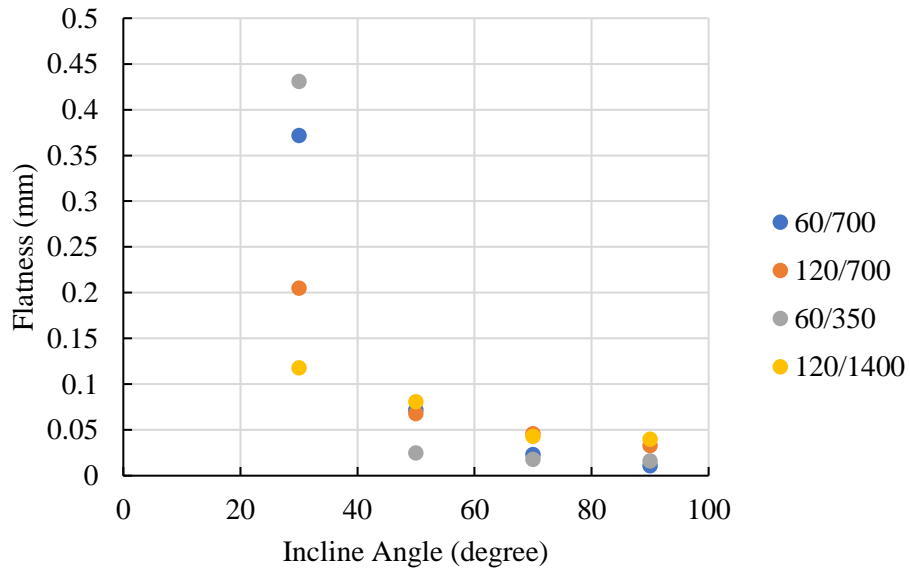
Figure 16. Flatness of the downface surfaces for contour sets 2 through 5 from the CMM program report.
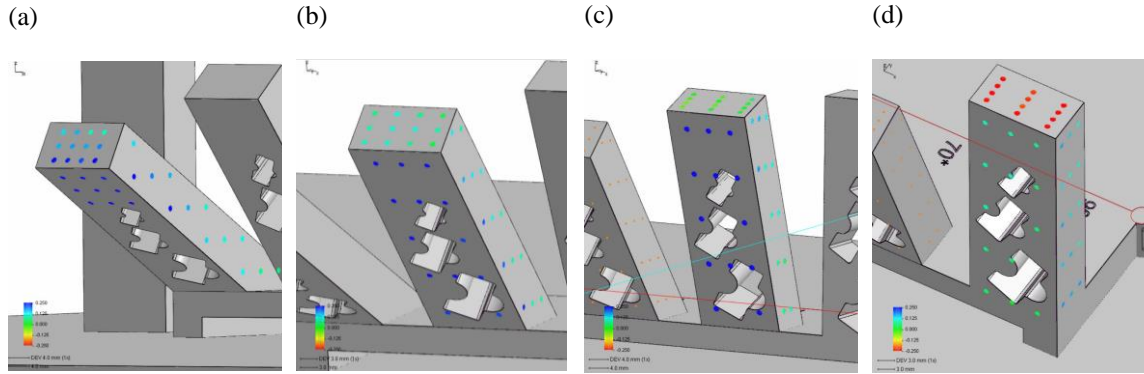
Figure 17. Point cloud color mapping of v2 overhang specimen at (a) 30°, (b) 50°, (c) 70°, and (d) 90°.

There is clear evidence that a relationship exists between the part geometry and the resulting dimensionality of fabricated parts. A connection between the laser power and scan speed also exists with the dimensional accuracy of overhanging surfaces. This evidence is initially shown through the CMM measurements of the thickness and width and verified through the point cloud color gradient and visible inspection.

EFFECT OF VARIATION IN BEAM OFFSET

A test to examine the effect of the contour beam offset in the dimensionality of the benchmark part was conducted early on with the initial overhang benchmark specimen and contour sets 1, and 2. The purpose of the beam offset is to help maintain dimensional accuracy of the supplied STL to the fabricated part. Adjusting the beam offset moves the center of the laser inward or outward from the part's contour. The typical offset value is around the radius of the melt pool diameter so the contour of the part matches with the edge of the melted material. The two beam offset settings each have the potential for two contour passes and the values are denoted as $1^{st}/2^{nd}$. The thickness and width measurement deviations from CAD for the two beam offset settings are shown in **Figure 18**.

22
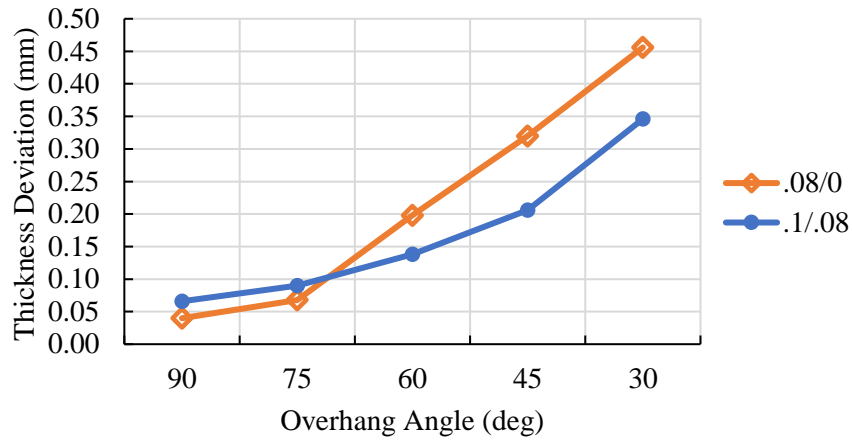
(a)
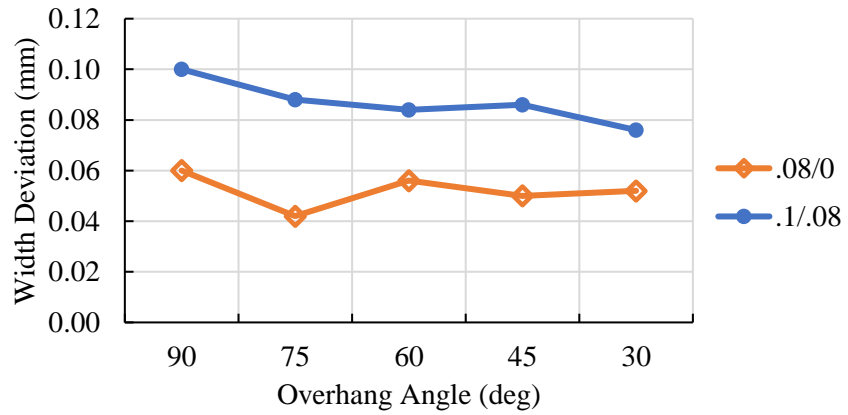
(b)

Figure 18. (a) Thickness and width measurement deviations of v1 specimen for beam offsets of 0.08/0 and 0.1/0.08.

While the effects of increasing the beam offset is clear in the width measurement, the separation of the two beam offset settings is closer in the thickness measurement. The increase in deviation from CAD was expected to occur for the thickness dimension, since the overhang bars were not supported. When comparing the effects of beam offset to the effects of laser power and scan speed, the beam offset changes resulted in a smaller deviation from the nominal feature sizes.

PLANAR SURFACES

For the planar surfaces, the surface roughness testing resulted in the same trend occurring for each of the tested contour laser power and scan speed bundles. The presence of a 3rd order polynomial trendline with similar amplitude values confirms the statement that the surface roughness of planar surfaces does not differentiate much between varying contour settings. The main control over surface roughness some from part geometry. Both relationships can be seen in **Figure 19**. The 30° downskin was not able to be measured due to the profilometer exceeding its measurable limits and is not shown in the figure. From the presence of the polynomial trendlines it is expected for the 30° downskin to exceed 40 μm *Ra*.
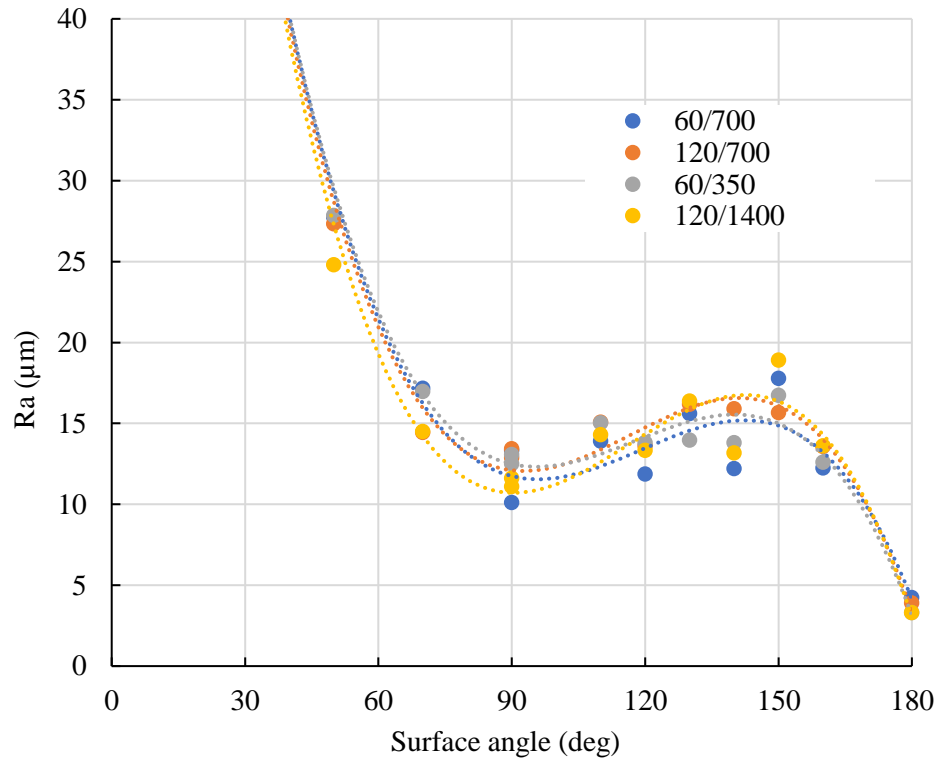
Figure 19. Surface roughness data for upface, downface, and topface surfaces of the v2 overhanging bar across contour sets 2 through 5.

CONCAVE AND CONVEX HOLES

The addition of the concave and convex holes provided insight into how unsupported features are affected by varying the build parameters and their location on an overhanging part. In regard to the varying the laser power and scan speed the surface roughness followed a similar trend across all parameter sets which is shown in **Figure 20b** for an overhang angle of 50° and measurement angle of 180° concave. The surface roughness across each angle was similar, however due to the measurement being of the 180° concave, the profilometer stylus was located on a section that was parallel to the build plate, resulting in a smaller roughness measurement from the absence of a layer line. Other than the occurrence for the 90° holes, there is a slight difference for the surface roughness of the holes in terms of incline angle. The 50° incline had the highest *Ra* values, but it should be noted that the difference between the other incline angles is within 5μm. When comparing the different radii, the 1mm radius has higher *Ra* values across all incline angles. This is due to the 90° incline having smaller surface roughness values for the 180° concave measurement. The surface roughness for all measurement angles, contour settings, and hole size can be found in the Appendix, **Table 8-11**.

(a)
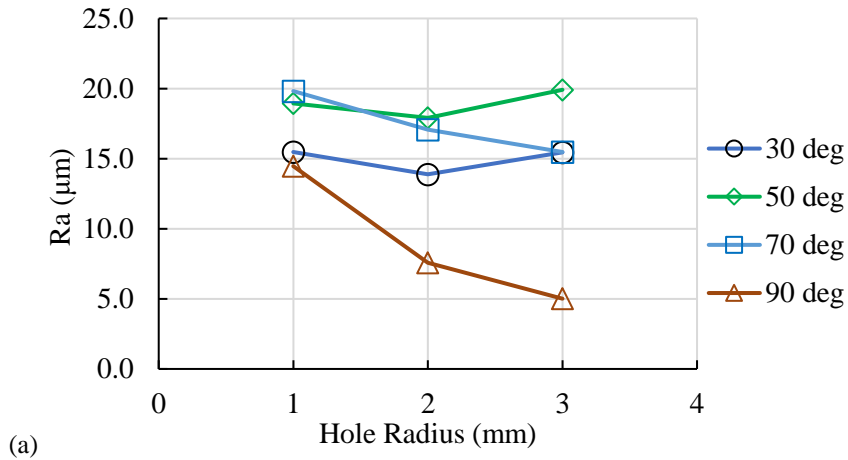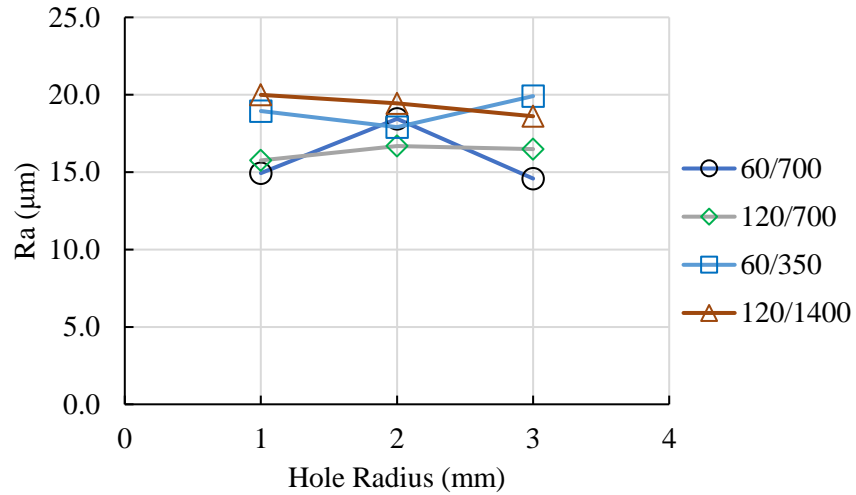
(b)

Figure 20. Effect on surface finish for hole features with (a) varying incline angle for a single parameter measured at 180° concave, and (b) varying parameter for a single incline angle at 50°.

The measurements between the two extremes for concave and convex surfaces follow a similar trend across all tested contour sets. The trend is that the measurements between the 90° and bottom measurement location have values that fit within the two extremes found at the outside measurement locations. **Figure 21** shows these trends for both (a) the concave and (b) convex measurement angles. The middle measurement locations were difficult to measure and therefore are not listed, however they are assumed to follow the same trend as the r2 and r3 measurements since the endpoints do.
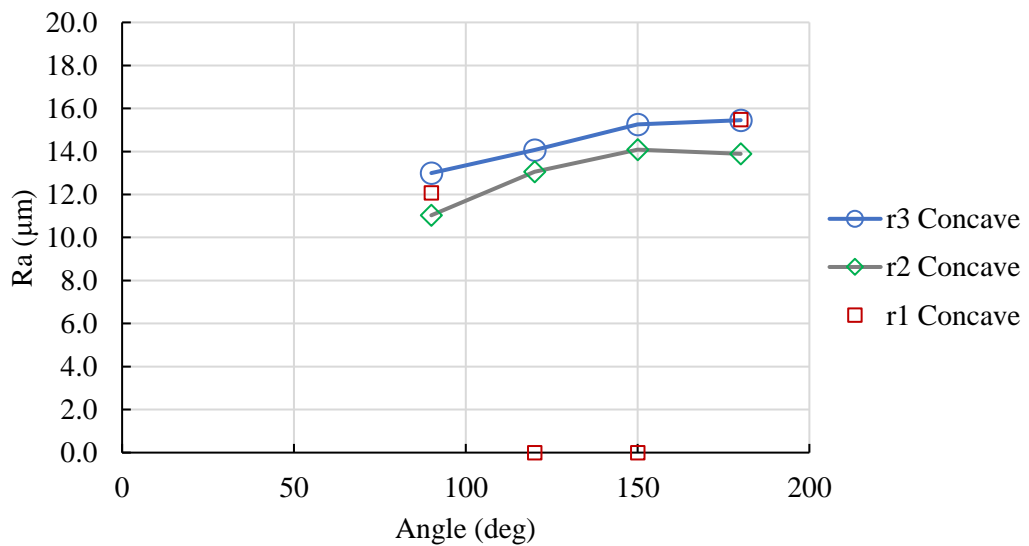
(a)
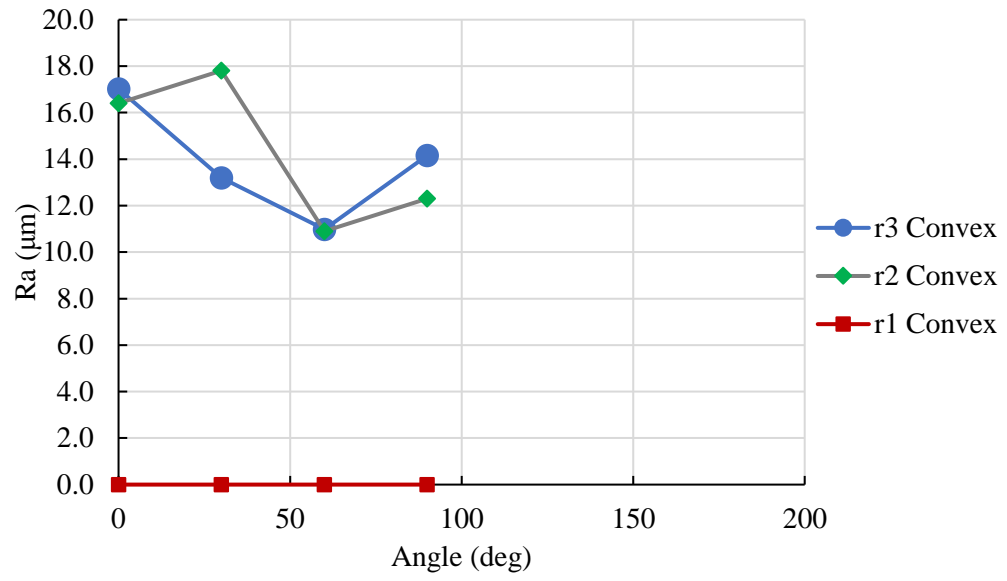
(b)

Figure 21. Concave (a) and convex (b) measurements for contour set 4.

CONCLUSIONS

Understanding the relationship that part geometry and parameter values have with the resulting dimensional accuracy and surface quality of SLM fabricated part is crucial to ensure the success of application parts. From literature it is know that the surface roughness and dimensional accuracy of SLM parts can be controlled through adjusting the fabrication parameters, scan strategy and part geometry. Focusing on the effects of contour parameter setting changes for surfaces and hole features on incline planes the individual connections of each variable to surface roughness and dimensionality through the fabrication of a single part design.

For varying contour laser power and scan speed settings there is a clear relationship as the two higher energy densities gave smaller the nominal dimensions while the lower energy density gave higher measured dimensions for the thickness and width measurements. Between surface roughness and dimensional accuracy, the contour parameters have a greater effect on dimensional accuracy. Adjusting not only the laser power and scan speed results in changes to the measured part dimensions, but so does the beam offset parameter.

The part geometry has a greater effect on surface roughness than dimensionality for both the planar surfaces and hole features. The trend for planar surfaces followed a 3rd order polynomial trend whereas the incline angle decreased to 30° the Ra would increase to where it could no longer be measured by the surface profilometer. This was different for the hole features, but both the concave and convex surfaces have the same trend. The side and bottom of each surface were the maximum and minimum Ra values for the radiused surface. The two measurements between the endpoints created an almost linear trend between the maximum and minimum measurements. In terms of dimensional accuracy, the closer the overhang surface got to 0°, the more sagging there was. This sagging was not only dependent on part geometry, but also on the contour settings. Based off visual inspection and the point cloud inspection reports for each specimen, shown in

28

Appendix A (**Figure 22**-**25)**, the sagging effect occurs for contour sets 2 and 4, which have the lowest power setting of 60W and slower scan speeds. The other two specimens do not have as severe sagging with a power setting of 120 W and have higher scan speeds.

Overall, a clear relationship between overhanging geometry and contour parameter settings and the dimensional accuracy and surface quality for parts fabricated in 17-4 stainless steel via SLM. Future work should include mechanical property testing of overhang specimens to determine if the incline angle influences mechanical properties. The presence of high surface roughness has been linked to controlling fatigue properties of SLM parts and further investigation of these effects would be beneficial in strengthening the significance of this current research work.

REFERENCES

Calignano, F., Peverini, O. A., Addamo, G., & Iuliano, L. (2020). Accuracy of complex internal channels produced by laser powder bed fusion process. *Journal of Manufacturing Processes, 54*, 48-53. doi:10.1016/j.jmapro.2020.02.045

Delgado, J., Ciurana, J., & Rodríguez, C. A. (2012). Influence of process parameters on part quality and mechanical properties for DMLS and SLM with iron-based materials. *The International Journal of Advanced Manufacturing Technology, 60*(5), 601-610. doi:10.1007/s00170-011-3643-5

Deng, Y., Mao, Z., Yang, N., Niu, X., & Lu, X. (2020). Collaborative Optimization of Density and Surface Roughness of 316L Stainless Steel in Selective Laser Melting. *Materials (Basel, Switzerland), 13*(7). doi:10.3390/ma13071601

DePond, P. J., Guss, G., Ly, S., Calta, N. P., Deane, D., Khairallah, S., & Matthews, M. J. (2018). In situ measurements of layer roughness during laser powder bed fusion additive manufacturing using low coherence scanning interferometry. *Materials & Design, 154*, 347-359. doi:10.1016/j.matdes.2018.05.050

Fox, J. C., Moylan, S. P., & Lane, B. M. (2016). Effect of process parameters on the surface roughness of overhanging structures in laser powder bed fusion additive manufacturing. In M. A. Davies & R. Msaoubi (Eds.), *3rd Cirp Conference on Surface Integrity* (Vol. 45, pp. 131-134). Amsterdam: Elsevier Science Bv.

Gockel, J., Sheridan, L., Koerper, B., & Whip, B. (2019). The influence of additive manufacturing processing parameters on surface roughness and fatigue life. *International Journal of Fatigue, 124*, 380-388. doi:10.1016/j.ijfatigue.2019.03.025

Klingaa, C., Dahmen, T., Baier, S., Mohanty, S., & Hattel, J. (2020). X-ray CT and image analysis methodology for local roughness characterization in cooling channels made by metal additive manufacturing. *Additive Manufacturing, 32*, 101032.

Mani, M., Lane, B. M., Donmez, M. A., Feng, S. C., & Moylan, S. P. (2017). A review on measurement science needs for real-time control of additive manufacturing metal powder bed fusion processes. *International Journal of Production Research, 55*(5), 1400-1418. doi:10.1080/00207543.2016.1223378

Ni, C., Shi, Y., & Liu, J. (2019). Effects of inclination angle on surface roughness and corrosion properties of selective laser melted 316L stainless steel. *Materials Research Express, 6*(3), 9. doi:10.1088/2053-1591/aaf2d3

Shi, W. T., Wang, P., Liu, Y. D., & Han, G. L. (2019). Experiment of Process Strategy of Selective Laser Melting Forming Metal Nonhorizontal Overhanging Structure. *Metals, 9*(4), 15. doi:10.3390/met9040385

Solberg, K., Guan, S., Razavi, S. M. J., Welo, T., Chan, K. C., & Berto, F. (2019). Fatigue of additively manufactured 316L stainless steel: The influence of porosity and surface roughness. *Fatigue & Fracture of Engineering Materials & Structures, 42*(9), 2043-2052. doi:10.1111/ffe.13077

Subbaian Kaliamoorthy, P., Subbiah, R., Bensingh, J., Kader, A., & Nayak, S. (2020). Benchmarking the complex geometric profiles, dimensional accuracy and surface analysis of printed parts. *Rapid Prototyping Journal, 26*(2), 319-329. doi:10.1108/rpj-01-2019-0024

Tran, H. C., & Lo, Y. L. (2019). Systematic approach for determining optimal processing parameters to produce parts with high density in selective laser melting process. *International Journal of Advanced Manufacturing Technology, 105*(10), 4443-4460. doi:10.1007/s00170-019-04517-0

Wang, D., Yang, Y., Yi, Z., & Su, X. (2013). Research on the fabricating quality optimization of the overhanging surface in SLM process. *The International Journal of Advanced Manufacturing Technology, 65*(9), 1471-1484. doi:10.1007/s00170-012-4271-4

Wohlers, T. T., Associates, W., Campbell, I., Caffrey, T., Diegel, O., & Kowen, J. (2018). *Wohlers Report 2018: 3D Printing and Additive Manufacturing State of the Industry : Annual Worldwide Progress Report*: Wohlers Associates

Raw data and measurement output reports for dimensionality for benchmark parts v1 and v2.

Table 5. CMM dimension measurements for contour sets 2 through 5, with power and speed settings noted, along with nominal values for both width and thickness of benchmark v2 overhang bars.

		Power (W)		60	120	60	120
		Speed (mm/s)		700	700	350	1400
	Energy Density (J/mm)	p/s		0.086	0.171	0.171	0.086
	Graph series notation:			60/700	120/700	60/350	120/1400
Overhang angle	Dimension	Nominal (mm)		Contour Set 2	Contour Set 3	Contour Set 4	Contour Set 5
90°	width	18		18.259	17.756	17.385	18.245
70°	width	18		18.312	17.736	17.337	18.287
50°	width	18		18.372	17.699	17.574	18.364
30°	width	18		18.312	17.523	17.443	18.333
90°	thick	10		10.287	9.869	9.694	10.312
70°	thick	10		10.239	9.367	9.463	10.214
50°	thick	10		10.384	9.813	9.812	10.413
30°	thick	10		9.804	9.609	9.345	10.205

Table 6. Measurement deviations from CAD for v1 benchmark part with varying beam offset settings.

	Contour Set	Beam Offset Settings (mm)	Run #	Overhang Angle				
				90°	75°	60°	45°	30°
Thickness Deviation	1	.08/0	1	0.06	0.06	0.18	0.31	0.45
			2	0.04	0.07	0.21	0.34	0.44
			3	0.02	0.09	0.17	0.31	0.48
			4	0.05	0.05	0.21	0.33	0.46
			5	0.03	0.07	0.22	0.31	0.45
	2	.1/.08	1	0.05	0.09	0.12	0.21	0.32
			2	0.06	0.08	0.14	0.23	0.37
			3	0.07	0.09	0.15	0.19	0.36
			4	0.09	0.1	0.13	0.2	0.33
			5	0.06	0.09	0.15	0.2	0.35
Width Deviation	1	.08/0	1	0.06	0.05	0.07	0.04	0.06
			2	0.06	0.03	0.06	0.06	0.05
			3	0.07	0.04	0.06	0.07	0.05
			4	0.05	0.03	0.06	0.04	0.06
			5	0.06	0.06	0.03	0.04	0.04
	2	.1/.08	1	0.12	0.09	0.09	0.09	0.07
			2	0.11	0.08	0.09	0.07	0.09
			3	0.08	0.09	0.09	0.11	0.07
			4	0.1	0.07	0.07	0.07	0.06
			5	0.09	0.11	0.08	0.09	0.09

(a)

(b)

(c)

(d)

(e)

(f)

(g)

(h)
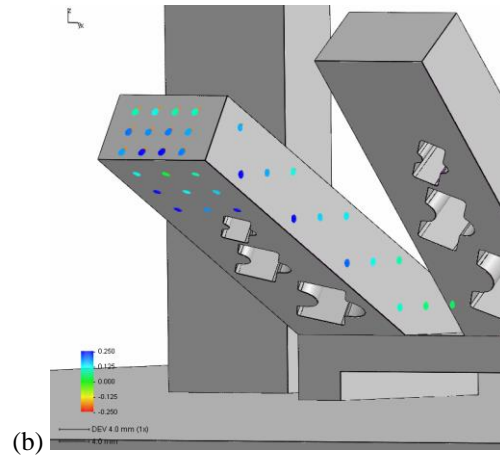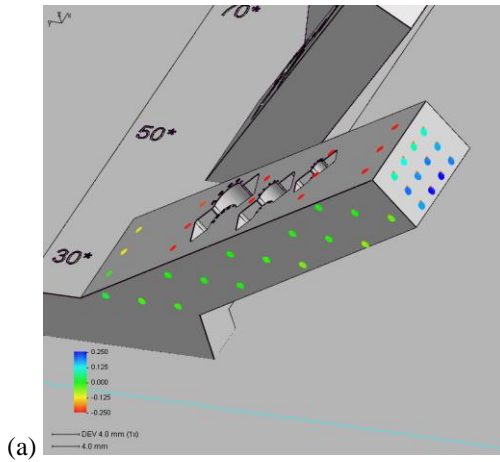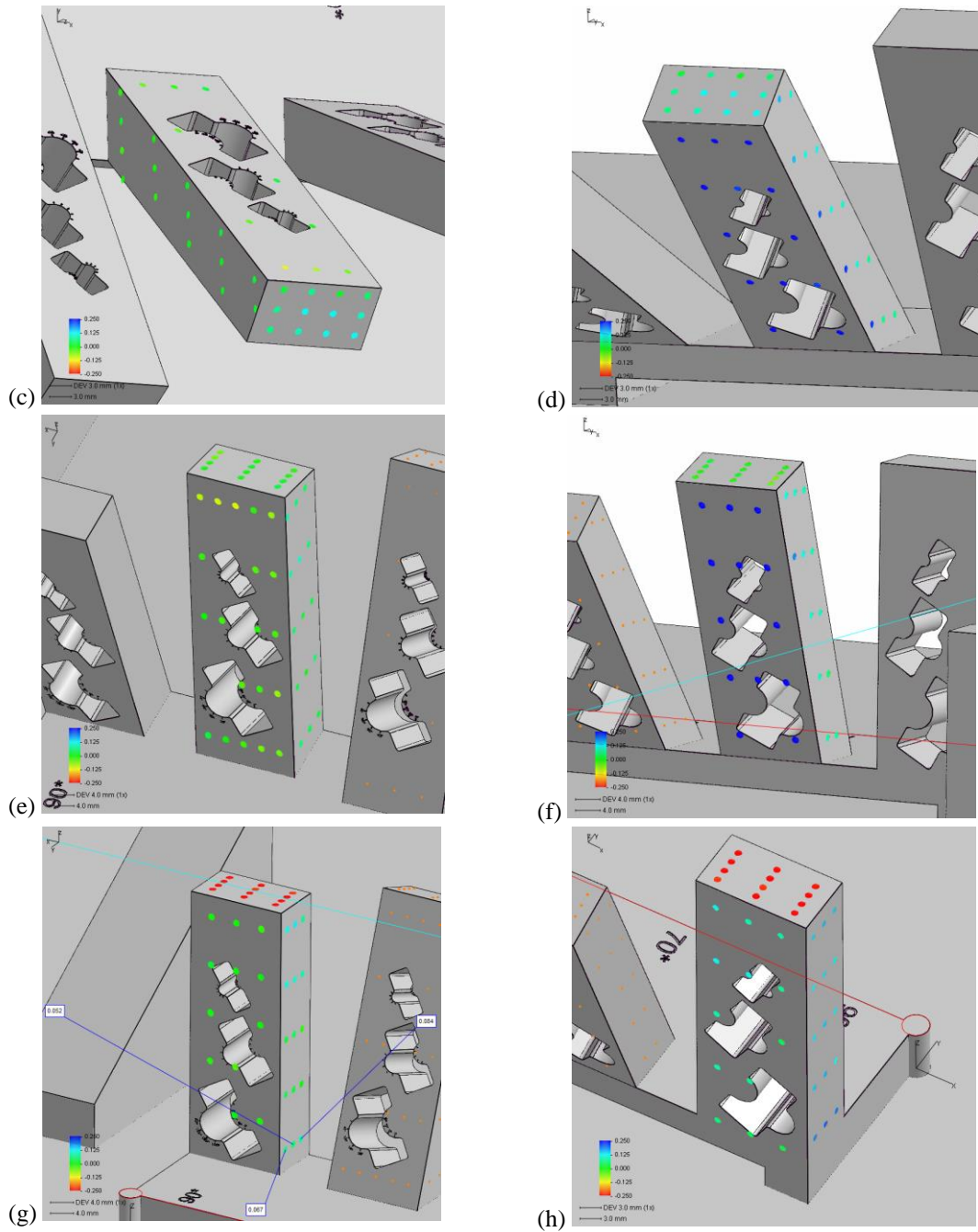
Figure 22. Point cloud visual display for contour set 2 with point cloud deviations at (a-b) 30° (c-d) 50°, (e-f) 70°, and (g-h) 90° overhang planes.

(g)

(h)
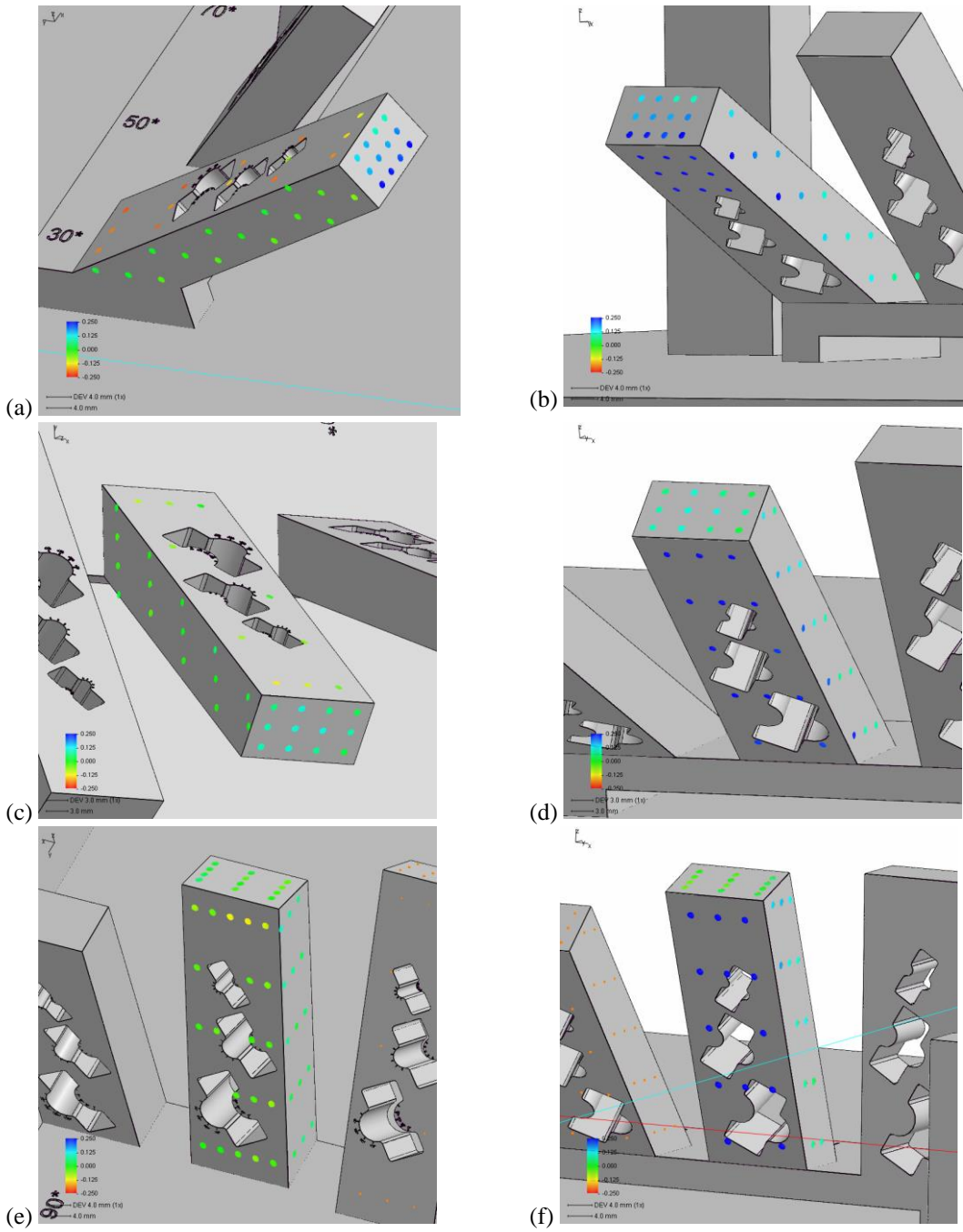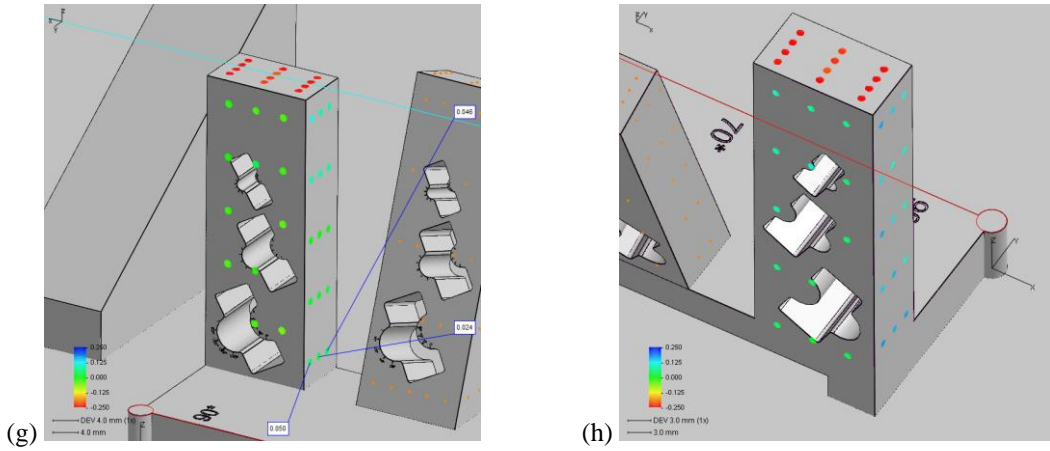
Figure 23. Point cloud visual display for contour set 3 with point cloud deviations at (a-b) 30° (c-d) 50°, (e-f) 70°, and (g-h) 90° overhang planes.

(a)

(b)

(c)

(d)
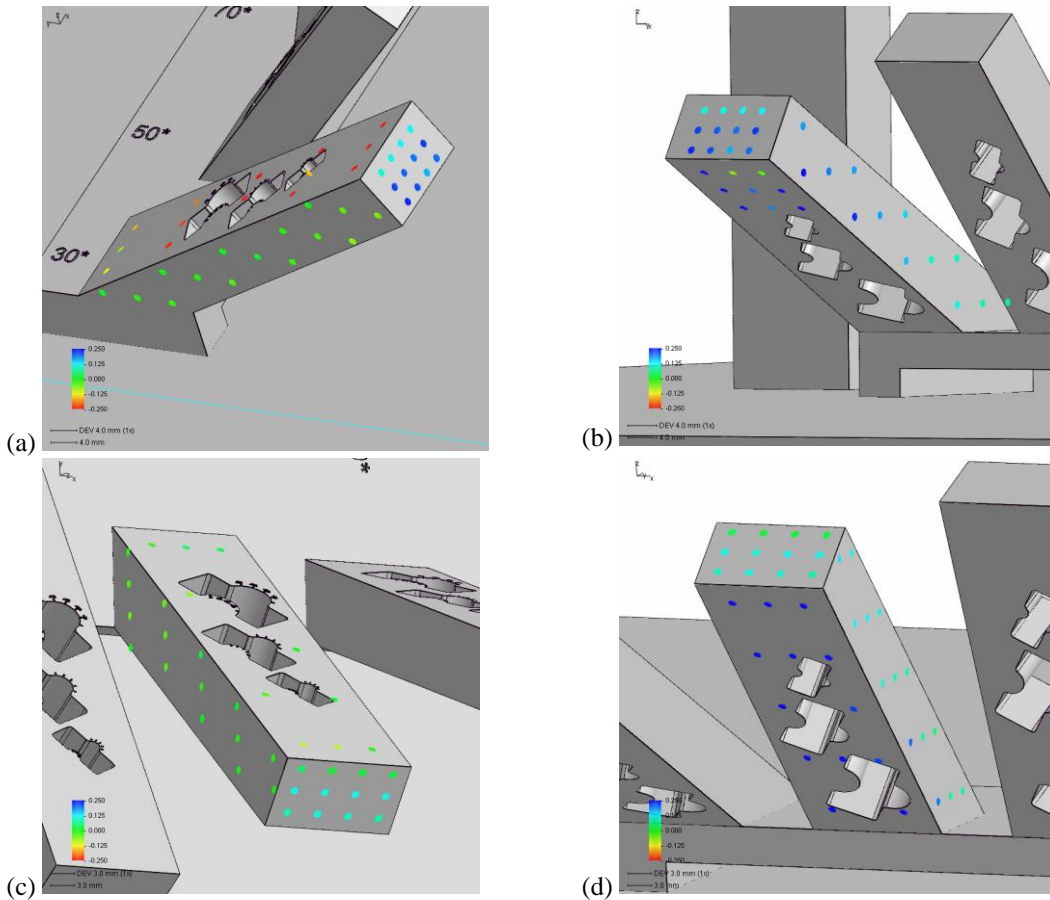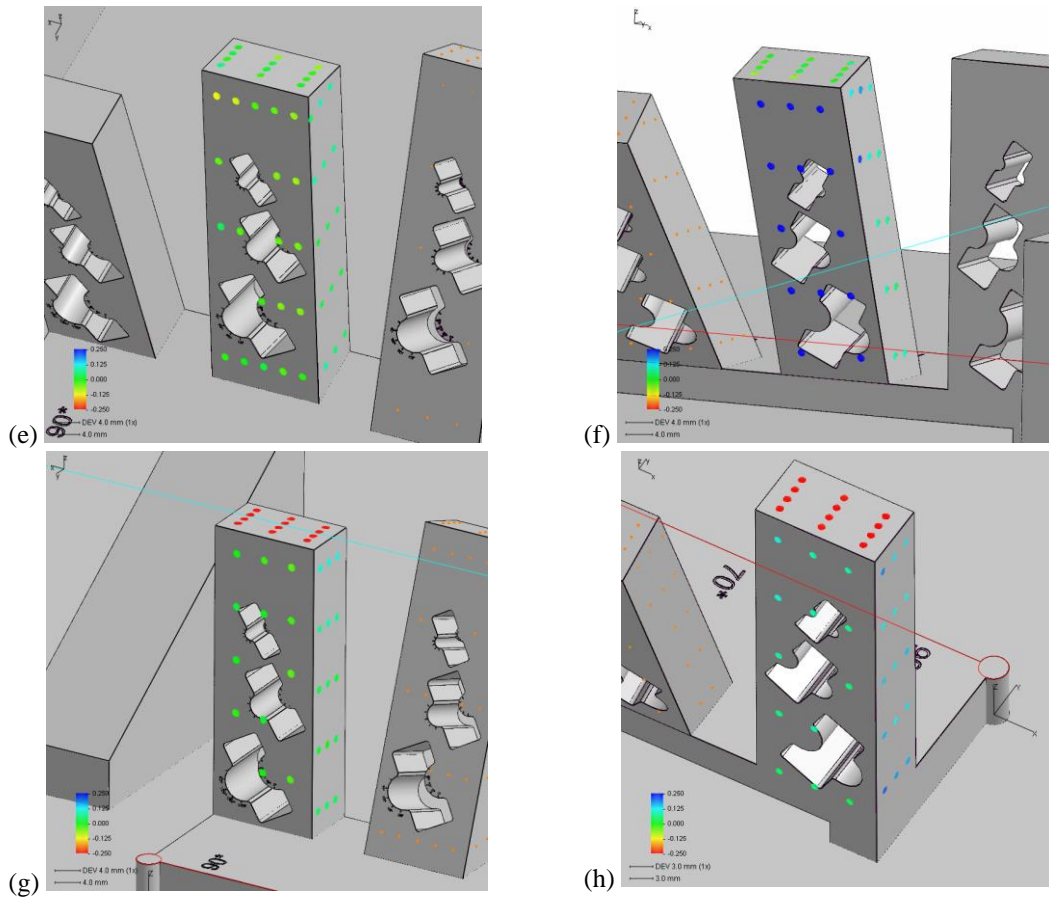
Figure 24. Point cloud visual display for contour set 4 with point cloud deviations at (a-b) 30° (c-d) 50°, (e-f) 70°, and (g-h) 90° overhang planes.
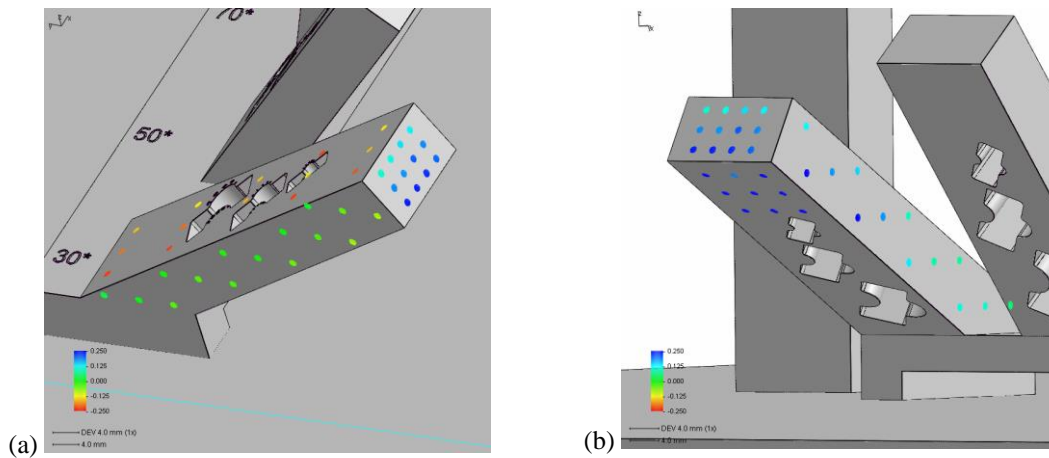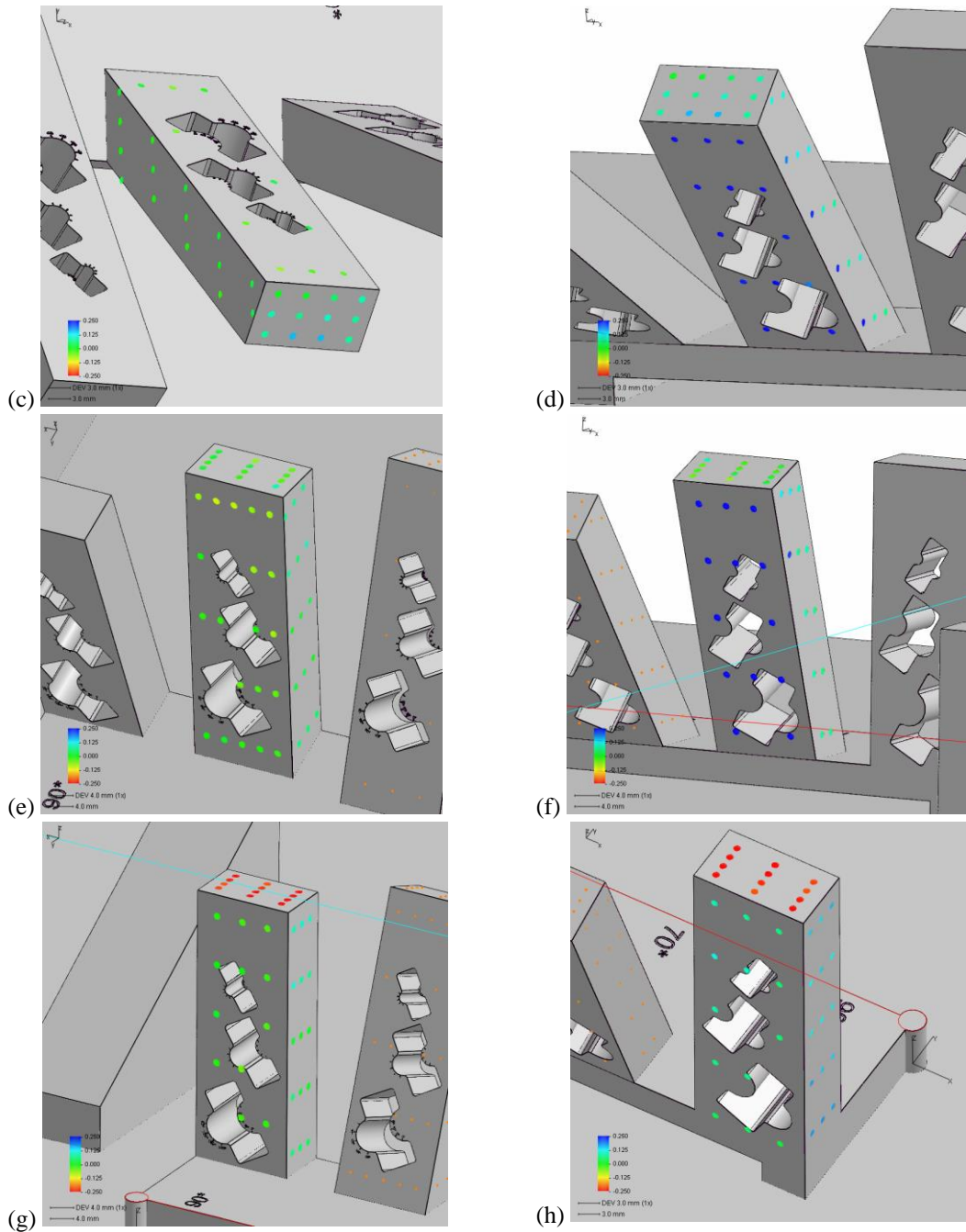
Figure 25. Point cloud visual display for contour set 5 with point cloud deviations at (a-b) 30° (c-d) 50°, (e-f) 70°, and (g-h) 90° overhang planes.

Table 7. Downface flatness callout from CMM program for contour sets 2 through 5 for all overhang bars on specimen.

Laser Power/ Scan Speed	60/700	120/700	60/350	120/1400
Overhang Angle	Block 1	Block 2	Block 3	Block 4
90	0.011	0.033	0.016	0.04
70	0.023	0.046	0.018	0.043
50	0.072	0.068	0.025	0.081
30	0.372	0.205	0.431	0.118

Organized raw data of surface roughness for benchmark part v2. A "-" symbolizes there is no data for that point due to the profilometer's inability to get a reading within its range, or there was no clear access point for the measurement location. The standard deviation and average for the three measurement runs are included in the tables.

Table 8. Surface profilometer measurements of *Ra* for each feature on benchmark specimen v2 built with contour set 2.

Feature			Ra (µm)				
Overhang Angle	Hole/Plane	Angle	Run 1	Run 3	Run 3	STD DEV	AVG
30	Upface	-	17.020	18.225	18.022	0.645	17.756
	Downface					-	-
	Topface		11.335	12.669	11.579	0.710	11.861
50	Upface	-	16.044	15.601	15.225	0.410	15.623
	Downface		25.069	31.656	26.393	3.484	27.706
	Topface		11.017	12.013	13.573	1.288	12.201
70	Upface	-	17.625	15.819	17.985	1.161	17.143
	Downface		14.494	14.041	13.222	0.645	13.919
	Topface		11.790	12.289	12.599	0.408	12.226
90	Upface	-	12.355	11.822	6.124	3.454	10.100
	Downface		13.245	12.869	13.699	0.416	13.271
	Topface		4.095	3.669	4.942	0.648	4.235
30	r3- concave	180	17.527	17.119	18.890	0.927	17.845
		150	16.564	15.791	14.273	1.166	15.543
		120	13.442	14.460	12.881	0.800	13.594
		90	11.943	12.806	11.419	0.700	12.056
	r3 – convex	0	15.486	17.292	15.112	1.166	15.963
		30	16.868	14.764	16.475	1.119	16.036
		60	11.169	11.763	11.191	0.337	11.374
		90	15.155	13.919	15.142	0.710	14.739
	r2- concave	180	13.643	15.723	13.306	1.309	14.224
		150	13.727	13.704	13.180	0.309	13.537
		120	13.567	12.195	13.607	0.804	13.123
		90	11.243	12.229	12.809	0.792	12.094
	r2 - convex	0	17.012	13.260	18.109	2.543	16.127
		30	15.210	14.212	17.274	1.562	15.565
		60	12.641	12.592	12.910	0.171	12.714
		90	14.714	14.459	14.751	0.159	14.641

		180	16.751	16.366	13.976	1.503	15.698
	r1- concave	150				-	-
		120				-	-
		90	11.416	13.811	15.000	1.826	13.409
		0				-	-
	r1 - convex	30				-	-
		60				-	-
		90				-	-
50		180	13.666	15.290	14.798	0.833	14.585
	r3- concave	150	19.050	17.622	17.036	1.036	17.903
		120	12.290	13.954	12.548	0.896	12.931
		90	13.762	13.224	14.421	0.600	13.802
		0				-	-
	r3 - convex	30	24.231	20.726	21.394	1.861	22.117
		60	15.800	15.136	16.330	0.598	15.755
		90	11.711	13.064	13.146	0.806	12.640
		180	18.424	17.806	19.111	0.653	18.447
	r2- concave	150	15.023	13.545	15.246	0.924	14.605
		120	12.099	13.178	13.005	0.580	12.761
		90	11.004	11.503	10.710	0.401	11.072
		0				-	-
	r2 - convex	30	23.173	22.519	22.111	0.536	22.601
		60	15.168	14.843	15.896	0.539	15.302
		90	13.509	13.067	11.651	0.971	12.742
		180	14.657	15.121	15.019	0.244	14.932
	r1- concave	150				-	-
		120				-	-
		90	17.963	17.757	18.218	0.231	17.979
		0				-	-
	r1 - convex	30	26.042			-	26.042
		60				-	-
		90				-	-
70		180	17.838	19.364	17.298	1.071	18.167
	r3- concave	150	24.636	15.930	22.335	4.511	20.967
		120	16.472	16.639	15.425	0.658	16.179
		90				-	-
		0				-	-
	r3 - convex	30				-	-
		60	11.316	11.316	13.553	1.292	12.062
		90	13.703	15.031	13.898	0.717	14.211
		180	15.161	15.579	15.511	0.224	15.417
	r2- concave	150	18.146	15.489	15.194	1.626	16.276
		120	14.325	13.965	13.566	0.380	13.952

		90	13.395	12.952	12.734	0.337	13.027
		0				-	-
	r2 - convex	30				-	-
		60	12.516	13.729	12.045	0.869	12.763
		90	11.432	11.316	14.024	1.531	12.257
		180	19.604	19.313	19.081	0.262	19.333
	r1- concave	150				-	-
		120				-	-
		90	13.067	13.835	16.024	1.534	14.309
		0				-	-
	r1 - convex	30				-	-
		60				-	-
		90				-	-
90		180	5.429	3.769	5.594	1.009	4.931
	r3- concave	150				-	-
		120				-	-
		90				-	-
		0				-	-
	r3 - convex	30				-	-
		60				-	-
		90				-	-
		180	7.725	18.405	17.691	5.971	14.607
	r2- concave	150	14.192	16.554	15.626	1.190	15.457
		120	16.504	17.186	19.393	1.510	17.694
		90	9.302	9.442	9.821	0.269	9.522
		0				-	-
	r2 - convex	30				-	-
		60	13.760	19.351	16.605	2.796	16.572
		90	11.937	12.892	10.823	1.036	11.884
		180	10.352	10.123	9.643	0.362	10.039
	r1- concave	150				-	-
		120				-	-
		90	17.253	12.876	17.876	2.725	16.002
		0				-	-
	r1 - convex	30				-	-
		60				-	-
		90				-	-

Table 9. Surface profilometer measurements of *Ra* for each feature on benchmark specimen v2 built with contour set 3.

Feature	Ra (µm)

Overhang Angle	Hole/Plane	Side & Angle	Run 1	Run 2	Run 3	STD DEV	AVG
30	Upface	-	12.955	15.806	18.146	2.600	15.636
	Downface					-	-
	Topface		11.370	15.612	13.843	2.131	13.608
50	Upface	-	15.820	16.405	16.262	0.305	16.162
	Downface		30.571	24.039	27.385	3.266	27.332
	Topface		11.643	15.539	20.636	4.510	15.939
70	Upface	-	14.416	16.100	14.703	0.901	15.073
	Downface		14.900	14.586	14.678	0.161	14.721
	Topface		13.457	14.881	12.365	1.262	13.568
90	Upface	-	12.594	14.319	11.660	1.349	12.858
	Downface		15.343	12.475	12.451	1.663	13.423
	Topface		4.056	4.585	2.776	0.930	3.806
30	r3- concave	180	16.039	15.723	14.538	0.791	15.433
		150	13.174	13.000	14.611	0.884	13.595
		120	11.514	11.601	12.305	0.434	11.807
		90	13.619	13.943	13.872	0.170	13.811
	r3 - convex	0	16.319	18.261	15.544	1.400	16.708
		30	15.734	15.940	15.179	0.394	15.618
		60	12.240	13.297	13.554	0.696	13.030
		90	15.481	15.043	13.919	0.806	14.814
	r2- concave	180	13.439	15.404	15.093	1.056	14.645
		150	11.425	10.859	11.840	0.492	11.375
		120	14.515	13.763	7.250	3.995	11.843
		90	12.246	12.058	11.972	0.140	12.092
	r2 - convex	0	14.629	15.372	15.277	0.404	15.093
		30	14.842	14.808	14.990	0.097	14.880
		60	14.008	13.092	13.573	0.458	13.558
		90	15.629	16.331	16.335	0.406	16.098
	r1- concave	180	17.412	16.463	16.555	0.523	16.810
		150	13.609	13.612	14.227	0.356	13.816
		120				-	-
		90	14.569	13.570	13.752	0.532	13.964
	r1 - convex	0	16.751	16.502	17.542	0.543	16.932
		30	14.498	16.164	12.667	1.749	14.443
		60	13.316	12.868	12.595	0.364	12.926
		90				-	-
50	r3- concave	180	15.592	16.595	17.269	0.844	16.485
		150	17.200	16.384	17.418	0.545	17.001
		120	14.854	16.546	15.156	0.902	15.519
		90	12.623	12.084	11.230	0.702	11.979
	r3 - convex	0	24.337	22.599	21.366	1.493	22.767

		30	25.668	21.204	23.486	2.232	23.453
		60	11.665	11.613	13.990	1.358	12.423
		90	11.990	13.192	14.061	1.040	13.081
	r2- concave	180	16.834	16.647	16.578	0.132	16.686
		150	18.940	18.940	17.592	0.778	18.491
		120	15.038	14.130	15.307	0.617	14.825
		90	11.059	12.185	12.226	0.662	11.823
	r2 - convex	0	21.267	19.043	19.954	1.118	20.088
		30	19.324	16.700	19.447	1.552	18.490
		60	12.513	11.886	13.365	0.742	12.588
		90	12.250	14.301	12.689	1.080	13.080
	r1- concave	180	15.859	15.485	15.933	0.240	15.759
		150	16.346	15.405	16.406	0.561	16.052
		120				-	-
		90	19.123	16.975	18.325	1.086	18.141
	r1 - convex	0	25.983	22.951	23.031	1.728	23.988
		30	17.470	17.208	16.050	0.756	16.909
		60				-	-
		90				-	-
70	r3- concave	180	15.010	14.529	16.339	0.938	15.293
		150	15.988	13.704	17.190	1.771	15.627
		120				-	-
		90				-	-
	r3 - convex	0				-	-
		30				-	-
		60				-	-
		90	10.244	11.219	11.046	0.520	10.836
	r2- concave	180	18.792	17.302	17.121	0.917	17.738
		150	15.564	15.014	15.446	0.290	15.341
		120	15.093	14.676	14.731	0.227	14.833
		90	13.632	13.098	14.650	0.788	13.793
	r2 - convex	0				-	-
		30	20.438	23.940	23.724	1.963	22.701
		60	12.973	15.649	14.236	1.339	14.286
		90	13.812	14.211	12.559	0.862	13.527
	r1- concave	180	17.302	17.084	16.993	0.159	17.126
		150				-	-
		120				-	-
		90	15.704	17.828	17.629	1.173	17.054
	r1 - convex	0				-	-
		30				-	-
		60				-	-
		90				-	-

Overhang Angle	Hole/Plane	Side & Angle	Run 1	Run 2	Run 3	STD DEV	AVG
90	r3- concave	180				-	-
		150				-	-
		120				-	-
		90				-	-
	r3 - convex	0				-	-
		30				-	-
		60				-	-
		90				-	-
	r2- concave	180	19.519	6.42	6.179	7.633233	10.706
		150	14.059	12.118	11.392	1.378855	12.523
		120	13.087	14.298	13.483	0.617463	13.62267
		90	13.029	11.638	11.017	1.030264	11.89467
	r2 - convex	0				-	-
		30				-	-
		60	27.395	13.481	15.147	7.598119	18.67433
		90	14.022	13.771	13.011	0.526422	13.60133
	r1- concave	180				-	-
		150				-	-
		120				-	-
		90	14.113	12.82	16.223	1.717768	14.38533
	r1 - convex	0				-	-
		30				-	-
		60				-	-
		90				-	-

Table 10. Surface profilometer measurements of *Ra* for each feature on benchmark specimen v2 built with contour set 4.

Feature			Ra (µm)				
Overhang Angle	Hole/Plane	Side & Angle	Run 1	Run 2	Run 3	STD DEV	AVG
30	Upface		16.389	15.776	18.040	1.171	16.735
	Downface	-				-	-
	Topface		14.763	13.324	13.321	0.832	13.803
50	Upface		8.183	18.454	15.228	5.253	13.955
	Downface	-	32.558	23.667	27.225	4.475	27.817
	Topface		15.443	11.598	14.410	1.990	13.817
70	Upface		14.964	14.717	15.425	0.359	15.035
	Downface	-	17.306	16.251	17.306	0.609	16.954
	Topface		12.778	9.888	15.136	2.628	12.601
90	Upface	-	12.304	11.678	13.541	0.948	12.508
	Downface		12.874	12.842	13.527	0.387	13.081

	Topface		3.087	2.644	4.274	0.843	3.335
30	r3- concave	180	15.980	15.200	15.180	0.456	15.453
		150	16.192	14.587	14.984	0.836	15.254
		120	13.664	14.621	13.898	0.499	14.061
		90	12.707	13.244	13.034	0.271	12.995
	r3 - convex	0	18.093	17.664	15.305	1.501	17.021
		30	13.837	12.527	13.227	0.656	13.197
		60	10.993	11.107	10.846	0.131	10.982
		90	13.838	13.541	15.113	0.835	14.164
	r2- concave	180	14.238	13.482	13.934	0.380	13.885
		150	13.765	13.676	14.809	0.630	14.083
		120	11.746	12.942	14.491	1.376	13.060
		90	12.330	10.023	10.746	1.180	11.033
	r2 - convex	0	16.391	16.257	16.573	0.159	16.407
		30	19.035	18.117	16.269	1.409	17.807
		60	10.687	10.835	11.180	0.253	10.901
		90	11.700	12.194	13.027	0.671	12.307
	r1- concave	180	15.554	15.746	15.124	0.318	15.475
		150				-	-
		120				-	-
		90	12.179	13.324	10.721	1.305	12.075
	r1 - convex	0				-	-
		30				-	-
		60				-	-
		90				-	-
50	r3- concave	180	20.408	20.435	18.894	0.882	19.912
		150	16.973	17.620	17.392	0.328	17.328
		120	15.688	17.703	16.826	1.010	16.739
		90	11.889	13.390	11.295	1.080	12.191
	r3 - convex	0	22.497	24.596	25.048	1.361	24.047
		30	17.643	17.082	19.144	1.066	17.956
		60	11.783	11.440	11.882	0.232	11.702
		90	13.901	14.743	15.954	1.032	14.866
	r2- concave	180	18.451	16.264	19.014	1.453	17.910
		150	16.198	16.886	20.335	2.217	17.806
		120	13.262	14.281	13.277	0.584	13.607
		90	11.105	10.336	10.424	0.421	10.622
	r2 - convex	0				-	-
		30	19.082	21.708	20.057	1.327	20.282
		60	12.499	13.786	14.722	1.116	13.669
		90	13.985	12.804	13.558	0.598	13.449
	r1- concave	180	18.429	20.043	18.369	0.950	18.947
		150				-	-

		120				-	-
		90	14.371	14.566	14.137	0.215	14.358
	r1 - convex	0	26.016	25.445	28.990	1.903	26.817
		30	20.020	19.638	18.529	0.774	19.396
		60				-	-
		90				-	-
70	r3- concave	180	16.238	14.125	16.070	1.174	15.478
		150	17.280	16.980	17.287	0.175	17.182
		120	13.136	13.531	16.110	1.615	14.259
		90	13.442	13.608	11.963	0.906	13.004
	r3 - convex	0				-	-
		30				-	-
		60				-	-
		90	10.980	11.035	9.352	0.956	10.456
	r2- concave	180	16.497	17.957	16.726	0.785	17.060
		150	15.923	17.777	15.089	1.376	16.263
		120	11.438	12.302	13.881	1.239	12.540
		90	10.494	11.771	10.642	0.698	10.969
	r2 - convex	0				-	-
		30	26.634	23.999	22.687	2.010	24.440
		60	18.667	18.596	18.623	0.036	18.629
		90	10.251	10.272	10.747	0.281	10.423
	r1- concave	180	19.396	20.733	19.333	0.791	19.821
		150				-	-
		120				-	-
		90	18.016	14.925	17.852	1.739	16.931
	r1 - convex	0				-	-
		30				-	-
		60				-	-
		90				-	-
90	r3- concave	180	6.011	4.721	4.304	0.890	5.012
		150				-	-
		120				-	-
		90				-	-
	r3 - convex	0				-	-
		30				-	-
		60				-	-
		90				-	-
	r2- concave	180	11.229	6.030	5.479	3.173	7.579
		150	13.275	15.191	19.914	3.417	16.127
		120	14.220	14.350	15.054	0.449	14.541
		90	11.540	10.619	10.595	0.539	10.918
	r2 - convex	0				-	-

Feature			Ra (µm)				
		30	23.795	19.996	30.120	5.114	24.637
		60	14.242	19.036	24.210	4.985	19.163
		90	12.856	15.867	11.671	2.163	13.465
	r1- concave	180	11.693	15.602	16.108	2.416	14.468
		150				-	-
		120				-	-
		90	10.814	10.931	11.344	0.278	11.030
	r1 - convex	0				-	-
		30				-	-
		60				-	-
		90				-	-

Table 11. Surface profilometer measurements of *Ra* for each feature on benchmark specimen v2 built with contour set 5.

Feature			Ra (µm)				
Overhang Angle	Hole/Plane	Side & Angle	Run 1	Run 2	Run 3	STD DEV	AVG
30	Upface	-	17.263	22.957	16.402	3.562	18.874
	Downface					-	-
	Topface		13.934	15.770	10.286	2.791	13.330
50	Upface	-	16.393	14.279	18.387	2.054	16.353
	Downface		23.592	27.598	23.206	2.432	24.799
	Topface		12.888	12.216	14.431	1.136	13.178
70	Upface	-	14.549	14.427	13.984	0.297	14.320
	Downface		16.580	12.599	14.289	1.998	14.489
	Topface		10.859	17.668	12.108	3.625	13.545
90	Upface	-	11.718	11.187	11.852	0.352	11.586
	Downface		10.727	9.761	12.750	1.525	11.079
	Topface		3.643	3.127	3.187	0.282	3.319
30	r3- concave	180	14.088	13.799	17.572	2.100	15.153
		150	14.760	16.105	17.048	1.150	15.971
		120	13.776	12.128	12.562	0.854	12.822
		90	14.137	13.460	13.500	0.380	13.699
	r3 - convex	0	14.272	13.869	14.565	0.349	14.235
		30	15.734	12.045	12.547	2.001	13.442
		60	11.561	11.576	11.548	0.014	11.562
		90	13.328	12.442	11.688	0.821	12.486
	r2- concave	180	17.820	17.148	17.718	0.362	17.562
		150	15.901	15.695	12.821	1.722	14.806
		120	12.893	13.101	12.994	0.104	12.996
		90	13.592	14.944	12.303	1.321	13.613

		0	16.009	16.592	17.085	0.539	16.562
	r2 - convex	30	14.248	14.577		0.233	14.413
		60	13.520	12.649	11.699	0.911	12.623
		90	15.368	15.986	15.986	0.357	15.780
	r1- concave	180	15.050	14.792	14.915	0.129	14.919
		150				-	-
		120				-	-
		90	13.032	12.294	12.177	0.464	12.501
	r1 - convex	0	16.651	16.582	16.435	0.110	16.556
		30	16.675	17.109	15.165	1.020	16.316
		60	11.278	11.656	11.954	0.339	11.629
		90				-	-
50	r3- concave	180	18.380	18.992	18.460	0.333	18.611
		150	18.148	17.228	15.892	1.134	17.089
		120	14.510	14.937	13.865	0.540	14.437
		90	12.623	12.351	12.932	0.291	12.635
	r3 - convex	0	24.725	23.729	25.665	0.968	24.706
		30	20.779	17.816	22.010	2.156	20.202
		60	12.079	16.424	12.786	2.331	13.763
		90	11.328	12.280	13.718	1.203	12.442
	r2- concave	180	20.994	20.009	17.354	1.883	19.452
		150	14.692	17.539	17.160	1.546	16.464
		120	13.103	12.526	13.308	0.405	12.979
		90	13.158	12.711	13.601	0.445	13.157
	r2 - convex	0	21.485	23.450		1.389	22.468
		30	24.799	21.277	23.338	1.769	23.138
		60	16.689	13.879	12.678	2.059	14.415
		90	12.129	11.497	12.225	0.396	11.950
	r1- concave	180	21.209	21.209	17.564	2.104	19.994
		150				-	-
		120				-	-
		90	16.577	16.546	16.829	0.155	16.651
	r1 - convex	0				-	-
		30	22.438	25.309	23.122	1.500	23.623
		60				-	-
		90				-	-
70	r3- concave	180	16.065	16.490	14.635	0.972	15.730
		150	14.313	18.284	16.028	1.992	16.208
		120	12.226	12.932	11.170	0.887	12.109
		90	10.796	11.586	10.513	0.556	10.965
	r3 - convex	0				-	-
		30				-	-
		60	12.676	11.970	9.791	1.504	11.479

		90	10.879	10.805	12.090	0.721	11.258
	r2- concave	180	14.877	15.079	19.735	2.748	16.564
		150	14.988	17.191	18.478	1.765	16.886
		120	14.133	13.177	13.997	0.517	13.769
		90	11.374	13.102	10.443	1.349	11.640
	r2 - convex	0				-	-
		30				-	-
		60	11.251	13.232	14.041	1.435	12.841
		90	11.399	11.875	11.063	0.408	11.446
	r1- concave	180	13.463	15.809	16.222	1.488	15.165
		150				-	-
		120				-	-
		90	18.940	21.134	21.132	1.266	20.402
	r1 - convex	0				-	-
		30	24.389	26.630	21.615	2.512	24.211
		60				-	-
		90				-	-
90	r3- concave	180	13.078	15.409	12.841	1.419	13.776
		150				-	-
		120				-	-
		90				-	-
	r3 - convex	0				-	-
		30				-	-
		60				-	-
		90				-	-
	r2- concave	180	5.412	6.496	6.360	0.591	6.089
		150	13.808	15.066	14.964	0.699	14.613
		120	16.347	10.989	11.220	3.029	12.852
		90	13.392	13.076	11.536	0.993	12.668
	r2 - convex	0				-	-
		30				-	-
		60	16.398	12.479	12.469	2.266	13.782
		90	10.040	12.048	12.645	1.365	11.578
	r1- concave	180	11.482	12.452	10.457	0.998	11.464
		150				-	-
		120				-	-
		90	18.701	19.966	18.360	0.846	19.009
	r1 - convex	0				-	-
		30	30.934	22.411	21.783	5.112	25.043
		60				-	-
		90				-	-

CURRICULUM VITAE

NAME: Katherine Grace Schneidau

ADDRESS: 1802 Integrity Way, Unit 102

Louisville, KY 40220

DOB: Rochester Hills, Michigan – July 9, 1996

EDUCATION
& TRAINING: B.S., Mechanical Engineering
University of Louisville
2016-2019

AWARDS: Guy E. Bordeau Scholarship – Additive Manufacturing Users' Group

2020

PROFESSIONAL SOCIETITES:

PUBLICATIONS:

NATIONAL MEETING PRESENTATIONS

REFERRED JOURNALS

BOOKS AND SYMPOSIA

INVITED PRESENTATIONS